MOLECULAR TRANSPORT AND STRUCTURE OF DNA IN A CONGESTED STATE

ZHU XIAOYING

NATIONAL UNIVERSITY OF SINGAPORE

2010

MOLECULAR TRANSPORT AND STRUCTURE OF DNA IN A CONGESTED STATE

ZHU XIAOYING

(Ph.D.)

A THESIS SUBMITTED

FOR THE DEGREE OF DOCTER OF PHILOSOPHY

DEPARTMENT OF PHYSICS

NATIONAL UNIVERSITY OF SINGAPORE

2010

Acknowledgement

First and foremost, I would like to thank my supervisor, A/P Johan R. C. van der Maarel for his superb guidance of conducting this research. I appreciate the opportunity for professional and personal growth as a graduate student in one of the top groups in Singapore.

General thanks are extended to all former and current members of Johan's Group for the pervasive spirit of cordial collaboration and the creative atmosphere that produced amazing achievements.

Special thanks go to Dai Liang for his selfless and fruitful discussion, Ng Siow Yee and Binu Kundukad for their precious collaborations.

Last but not least, acknowledgement must go to my family for their continuous support and sharing, both in storm and sunshine.

List of Publications

1. Viscoelasticity of entangled lambda-phage DNA solutions

   ***Xiaoying Zhu**, Kundukad Binu, Johan R.C. van der Maarel*

   Journal of Chemical Physics, 129: 185103 (2008)

2. Effect of crowding on the conformation of interwound DNA strands from neutron scattering measurements and Monte Carlo simulations

   ***Xiaoying Zhu**, Siow Yee Ng, Amar Nath Gupta, Yuan Ping Feng, Bow Ho, Alain Lapp, Stefan U. Egelhaaf, V. Trevor Forsyth, Michael Haertlein, Martine Moulin, Ralf Schweins, and Johan R.C. van der Maarel*

   Physical Review E, 81: 061905 (2010)

Table of Contents

Summary

In this thesis, the molecular transportation properties and the structure of supercoiled DNA is investigated. To study dynamic properties of DNA, the viscoelastic moduli of lambda phage DNA through the entanglement transition were obtained with particle tracking microrheology. The number of entanglements per chain is obtained. The longest, global relaxation time pertaining to the motion of the DNA molecules is obtained as well. A comprehensive characterization of viscoelasticity of DNA solutions with increasing concentration in terms of viscous loss and elastic storage moduli is explored.

With a view to determining the distance between the two opposing duplexes in supercoiled DNA, small angle neutron scattering from pHSG298 plasmid dispersed in saline solutions were measured. Experiments were carried out under full and zero average DNA neutron scattering contrast for the first time. It was observed that the interduplex distance decreases with increasing concentration of salt as well as plasmid. Therefore, besides ionic strength, DNA crowding is shown to be important in controlling the interwound structure and site juxtaposition of distal segments of supercoiled DNA.

LIST OF TABLES

LIST OF FIGURES

Chapter 1

Introduction

1.1 Biomolecules in crowded conditions

Living cells contain a variety of biomolecules including nucleic acids, proteins, polysaccharides, metabolites as well as other soluble and insoluble components. These bio-molecules occupy a significant fraction (20-40%) of the cellular volume, leading to a crowded intracellular environment. This is commonly referred to as molecular crowding (1). Therefore, an understanding of the effects on bio-molecules in molecular crowded conditions is important to broad research fields such as biochemical, medical, and pharmaceutical sciences. However, the effects of molecular crowding on the properties of biomolecules are unclear. There is increasing interest in crowding on the structure, stability and transportation of biomolecules, in order to clarify how biomolecules behave in physiological conditions (2, 3).

Known as 'the blueprint of life' DNA plays an important role in many biological processes, such as replication, recombination, and transcription of the genome (4，5). DNA is often in crowded conditions and condensed into compact structures (6, 7, 8). Compaction and condensation are fundamental

properties of DNA, because in a living mammalian cell, it is compacted in length by a factor of as much as one million in order to be stored in a nucleus with only a 10-μm diameter.

When accommodated in a congested state, such as inside the nucleoid of a bacterial cell, DNA has to decrease its physical extent by changes in structure. Experiments in vitro have shown that in controlling the three dimensional conformation of closed circular DNA, the medium which supports DNA is of paramount importance (9, 10). The ionic strength of the supporting medium provides different screening conditions of DNA. From a biophysical point of view, it is of interest to understand the interplay between conformation and interactions in topologically constrained bio-molecules.

1.2 DNA supercoiling

In order to carry out various functions in biology, a DNA molecule must twist or untwist, and curve. DNA supercoiling, which allows DNA compaction into a very small volume, is an attribute of almost all DNA in vivo (11). Importantly, DNA supercoiling has a significant influence on DNA-associated processes, involving the interaction of specific proteins with DNA. Previous investigations show that the binding of proteins to DNA is often supercoiling dependent (12, 13).

There are two general varieties of DNA supercoiling. Known as toroidal,

the DNA coils into a series of spirals about an imaginary toroid or ring. The other is the plectonemic (or interwound) conformation in which the DNA crosses over and under another part of the same molecule repeatedly to form a higher order helix. The number of times the two strands of DNA double helix are rotated before closing to form a ring is called the linking number deficit. The linking number of deficit is a constant that can be changed only by breaking the DNA backbone. There are positive and negative supercoilings of plectonemic conformation. In vivo most DNAs are negatively supercoiled, that is they have a negative linking difference (14). Negative supercoiling is important for a wide variety of biological processes (15, 16, 17, 18, 19).

Supercoiled DNA can be visualized by (cryo-) electron and atomic force microscopy (9, 10, 20, 21). The shape of the molecule is observed to be quite irregular. However, the interduplex distance, which is the average distance between the opposing duplexes in the supercoil, is inversely proportional to the superhelical density and decreases with increased ionic strength of the supporting medium. These visualization techniques provide direct evidence of supercoiling of DNA, but are never without some ambiguity. Firstly, these imaging techniques can not be carried out in solution. In other words, it is difficult to preserve the environmental conditions. Secondly, there is always a possible effect of the spreading interface on the molecular confirmation (22).

The three-dimensional tertiary structure of DNA is determined by topological and geometric properties such as the degree of interwinding and

number of interwound branches. The topological constraint sets the spatial extent of the molecule and determines its excluded volume. Such topological and geometric properties (typical size-related properties) are best and quantitatively inferred from scattering experiments, because the electrostatic interaction modified by the ionic strength and the concentration of DNA can be adjusted in the condition of the solution. The interwound structure was observed in small angle neutron scattering work on supercoiled DNA either in dilute solution (23) or in liquid crystalline environment (24, 25). Zakharova et al obtained a pitch angle of around $55°$. A radius r and a pitch $2\pi p$ in the range 5-10 and 38-132 *nm* depending on DNA concentration were also derived (25). These experiments may however be compromised by the contribution to the scattering from inter-DNA interference; in particular those involving samples with higher plasmid and/or lower salt concentrations. Inter-DNA interference may obscure the information on the conformation. However, this inter-DNA interference can be eliminated by performing SANS experiments in the condition of zero average DNA contrast.

1.3 Viscoelasticity of DNA solutions

Bio-molecules are in crowded (or congested) conditions move unexpectedly fast. Since it is difficult to access the dynamical properties of DNA in cellular environment, studies in vitro provide valuable insight of the

behavior of DNA in vivo. Expressions for some molecular transport properties, i.e. the polymer self-diffusion coefficient and the viscosity were derived (26, 27, 28). Dynamics in the semi-dilute regime has also been discussed by de Gennes (26). Here, the dynamics is strongly affected by the chain overlap and the possible formation of transient, topological constraints. Hence a viable approach to investigate molecular transport properties is to explore the viscoelasticity of DNA solutions with increasing DNA concentration through the entanglement transition. Subsequent sections will provide an overview of viscoelasticity of biopolymers especially DNA.

1.3.1 Polymer dynamics from the dilute to the semi-dilute regime

If a polymer is dissolved in a suitable solvent and if the concentration is sufficiently low so that the average inter-coil distance far exceeds the size of the coil given by the Flory radius R_F, a dilute solution of coils can be obtained. In the diluted regime, DNA molecules can move freely as random coils, which are independent and non-interpenetrating. As the DNA concentration is increased above a critical overlap concentration, the molecules interpenetrate. Hence individual coils are no longer discernible and the so-called semi-dilute regime is formed. The overlap concentration is dependent on the persistence length and the contour length of the molecules. The thermodynamics and

chain statistics in the semi-dilute regime can be analyzed with scaling concepts. Scaling in polymer physics is based on the existence of a certain, unique length scale within which the chain is unperturbed by external factors.

In general, in order to obtain entanglements a certain number of chains *n* have to overlap. When the DNA concentration reaches about ten times higher than the overlap concentration, DNA chains become entangled and a transient elastic network is formed. Entanglements are topological constraints resulting from the fact that the DNA molecules cannot cross each other.

Polymer dynamics under entangled conditions can be described by reptation model, in which the polymer is thought to have a snake-like motion along the axial line (primitive path) in a confined tube which is formed by the entanglements (26). The reptation model gives specific scaling laws for the longest, global relaxation time, self-diffusion coefficient, high frequency limiting value of the elastic storage modulus, and the zero shear limit of the viscosity of neutral polymers in the entangled regime. The **tube like motion** of a single, flexible DNA molecule, which can be described by the reptation model, was visualized by fluorescence microscopy (29). Reptation of entangled DNA has been observed by Smith *et al*. as well (30). They measured the diffusion coefficient as a function of the concentration by tracking the Brownian motion of the DNA molecules with fluorescence microscopy. The self-diffusion coefficient decreases with increasing concentration according to $D \sim c^{-7/4}$ for a DNA concentration exceeding 0.5 g/L. These results comply

with reptation dynamics of a salted polyelectrolyte and indicate that the phage λ-DNA (which was used in their experiment) becomes entangled at 0.6 g of DNA/L, which is about 20 times the overlap concentration.

Musti et al. (31) reported low shear viscosity and relaxation times of solutions of T2-DNA (164kbp, contour length of 56 um). It was shown that the reduced zero shear viscosity obeys the same scaling law as the one for synthetic, linear polymers. The entanglement concentration of such T2-DNA is found to be 0.25g of DNA/L, whereas Smith et al. reported that the entanglement concentration of phage λ-DNA is around 0.6g of DNA/L. This difference is due to the lower molecular weight of λ-DNA compared to the one of T2-DNA.

1.4 Video-particle tracking method

The method of video particle tracking is based on the observation of trajectories of individual or multiple particles embedded in various solutions. By monitoring the Brownian motion of individual particles, one can derive local (micro)-rheological properties and resolve microheterogeneities of complex fluids (32, 33, 34, 35). Video-particle tracking provides a powerful approach to study biological samples especially when small quantities are available. Usually it requires only 5-100 micro-liters per sample. Particle tracking was introduced by Mason et al. in order to measure the viscoelastic

moduli of complex fluids by detection of thermally excited colloidal probe spheres suspended in the fluid (36, 37, 38). A phenomenological generalized Stokes-Einstein (GSE) equation was proposed. It was based upon the assumption that the complex fluid can be treated as a continuum around a sphere, or equivalently, that the length scales of the solution structures giving rise to the viscoelasticity are smaller than the size of the sphere. This GSE equation has been tested by comparing moduli obtained from Diffusing Wave Spectroscopy measurements and mechanical rheometry with consistency. Furthermore, Goodman et al. used the method of multiple-particle tracking to measure the microviscosity and degree of heterogeneity of solutions of DNA over a wide range of concentration and lengths to identify some of the topological parameters that affect DNA viscoelasticity (34).

1.5 Research objectives

When accommodated in a congested state, DNA has to decrease its physical extent by changing its conformation. To form a higher order helix, DNA often exists in a supercoiled form. Therefore, it is of importance to understand the conformation change of supercoiled DNA in crowded as well as in different environmental conditions such as the ionic strength. The effect of intermolecular interaction among DNA molecules at high concentrations and the interplay of ionic strength and DNA concentration also need to be

investigated.

As a result of increasing DNA concentration, the transport properties of the DNA molecules are different from the ones in dilute solutions. In this thesis, transport of DNA and its effect on the properties of the flow are investigated.

Specifically, this thesis covers

1) Investigation of viscoelasticity of phage λ-DNA from the dilute to the semi-dilute, entangled regime with the help of the video particle tracking method. The number of entanglements per chain is obtained. The longest, global relaxation time pertaining to the motion of the DNA molecules is obtained as well. A comprehensive characterization of the viscoelasticity of DNA solutions with increasing concentration in terms of the viscous loss and elastic storage moduli is presented.
2) In the conditions of full and zero average DNA contrast, small angle neutron scattering from pHSG298 plasmid (2675 base-pairs) was measured to determine the distance between the two opposing duplexes in supercoiled DNA. The availability of perdeuterated plasmid made the study of zero average DNA contrast possible for the first time. In the condition of zero average contrast, the scattering intensity is directly proportional to the statistically averaged single DNA molecule scattering (form factor) of DNA molecule, without complications from intermolecular interference.

The detailed study of these two topics is discussed in chapter 3 and 4,

respectively. Methodology for these studies, including sample preparation, sample characterization, and small angle neutron scattering is described in chapter 2.

References

1. Alberts, B., Bray, D., Lewis, J., Raff, M., Roberts, K. and Watson, J. D. 1995. Molecular Biology of the Cell, Newton Press, pp. 336–396.

2. Lukacs, G.L., Haggie, P., Seksek, O., Lechardeur, D., Freedman, N. and Verkman, A. S. 2000. Size-dependent DNA mobility in cytoplasm and nucleus, J. Biol. Chem. 275: 1625-1629.

3. J. Li, J.J. Correia, L. Wang, J.O. Trent, J.B. Chaires. 2005. Not so crystal clear: The structure of the human telomere G-quadruplex in solution differs from that present in a crystal, Nucleic Acids Res 33: 4649-4659.

4. Felsenfeld, G. 1996. Chromatin unfolds. Cell 86: 13-19.

5. Friedman, J. and Razin, A., 1976. Studies on the biological role of DNA methylation. II. Role of phiX174 DNA methylation in the process of viral progeny DNA synthesis. Nucleic Acids Res 3: 2665-2675.

6. Evdokimov Iu, M., Akimenko, N. M., Kadykov, V. A., Vengerov, IuIu. and Piatigorskaia, T. L. 1976. DNA compact form. VI. Changes of DNA secondary structure under conditions preceding its compaction in a solution. Mol Biol 10: 657-663.

7. Porter, I.M., Khoudoli, G.A. and Swedlow, J.R., 2004. Chromosome

condensation: DNA compaction in real time. Curr Biol 14: R554-556.

8. Guerra, R.F., Imperadori, L., Mantovani, R., Dunlap, D. D. and Finzi, L. 2007. DNA compaction by the nuclear factor-Y. Biophys J 93: 176-182.

9. Bednar, J., Furrer, P., Stasiak, A., Dubochet, J., Egelman, E. H. and Bates, A. D. 1994. The twist, writhe and overall shape of supercoiled DNA change during counterion-induced transition from a lossely to a tightly interwound superhelix. Possible implications for DNA structure in vivo. J Mol Biol 235: 825-847.

10. Boles, T.C., White, J.H. and Cozzarelli, N.R., 1990. Structure of plectonemically supercoiled DNA. J Mol Biol 213: 931-951.

11. A. D. Bates and A. Maxwell. 2005. DNA topology. Oxford University Press, Oxford.

12. Clark, D.J. and Leblanc, B. 2009. Analysis of DNA supercoiling induced by DNA-protein interactions. Methods Mol Biol 543: 523-535.

13. Butler, A.P. 1986. Supercoil-dependent recognition of specific DNA sites by chromosomal protein HMG 2. Biochem Biophys Res Commun 138: 910-916.

14. Worcel, A., Strogatz, S. and Riley, D., 1981. Structure of chromatin and the linking number of DNA. Proc Natl Acad Sci U S A 78:

1461-1465.

15. Benjamin, H. W. and Cozzarelli, N. R. 1990. Geometric arrangements of Tn3 resolvase sites. J. Biol. Chem 265: 6441-6447.

16. Funnell, B. E., Baker, T. A and Kornberg, A. 1986. Complete enzymatic replication of plasmids containing the origin of the E.Coli chromosome. J. Biol. Chem 261: 5616-5624.

17. McClure, W. R. 1985. Mechanism and control of transcription initiation in prokaryotes. Annu. Rev. Biochem 54: 171-204.

18. Salvo, J. J. and Grindley, N. D. F. 1988. The gamma delta resolvase bends the res site into a recombinogenic complex. EMBO J. 7: 3609-3616.

19. Kanaar, R., van de Putte, P. and Cozzarelli, N. R. 1989. Gin-mediated recombination of catenated and knotted DNA substrates: Implications for the mechanism of interaction between cis-acting sites. Cell 58: 147-159.

20. Lyubchenko, Y.L. and Shlyakhtenko, L.S. 1997. Visualization of supercoiled DNA with atomic force microscopy in situ. Proc Natl Acad Sci U S A 94: 496-501.

21. Zakharova, S.S., Jesse, W., Backendorf, C. and van der Maarel J. R. C. 2002. Liquid crystal formation in supercoiled DNA solutions. Biophys J 83: 1119-1129.

22. Ueda, M., Kawai, T., Iwasaki, H. 1998. Conformations of long

deoxyribonucleic acid molecule on silicon surface observed by atomic force microscopy. Japanese Jorunal of Applied Physics. 37: 3506-3507.

23. Hammermann, M., N. Brun, K. V. Klenin, R. May, K. Toth and J. Langowski. 1998. Salt-dependent DNA superhelix diameter studied by small angle neutron scattering measurements and Monte-Carlo simulations. Biophys. J 75: 3057-3063.

24. Torbet, J., and E. DiCapua. 1989. Supercoiled DNA is interwound in liquid-crystalline solutions. EMBO J 76: 2502-2519.

25. Zakharova, S. S., Jesse, W., Backendorf, C., Egelhaaf, S. U., Lapp, A. and J. R. C. van der Maarel. 2002. Dimensions of plectonemically supercoiled DNA. Biophys J 83: 1106-1108.

26. P. G. de Gennes, 1979. Scaling Concepts in Polymer Physics. Cornell University Press, Ithaca, NY.

27. J. R. C. van der Maarel. 2008 Introduction to Biopolymer Physics. World Scientific, Singapore.

28. M. Doi and S. F. Edwards, 1986. The theory of polymer dynamics. Oxford University Press.

29. Perkins, T. T., Quake, S. R., Smith, D. E., and Chu, S. 1994. Relaxation of a single DNA molecule observed by optical microscopy. Science 264: 822-826.

30. Smith, D. E., Perkins, T. T. and Chu, S. 1995. Self-diffusion of an

entangled DNA molecule by reptation. Phys Rev Lett 75: 4146-4149.

31. R. Musti, J. L. Sikorav, D. Lairiez, G. Jannink, and M. Adam. 1995. Viscoelastic properties of entangled DNA solutions. C. R. Acad. Sci. Paris 320: 599-604.

32. Anselmi, C., DeSantis, P. and Scipioni, A. 2005. Nanoscale mechanical and dynamical properties of DNA single molecules. Biophys Chem 113: 209-221.

33. Kealley, C. S., Sokolova, A. V., Kearley, G. J., Kemner, E., Russina, M., Faraone, A., Hamilton, W. A., and Gilbert, E. P. 2009. Dynamical transition in a large globular protein: Macroscopic properties and glass transition. Biochim Biophys Acta 1804: 34-40.

34. Goodman, A., Tseng, Y., and Wirtz, D. 2002. Effect of length, topology, and concentration on the microviscosity and microheterogeneity of DNA solutions. J Mol Biol 323: 199-215.

35. Tseng, Y., Kole, T. P. and Wirtz, D. 2002. Micromechanical Mapping of Live Cells by Multiple-Particle-Tracking Microrheology. Biophys J 83: 3162–3176.

36. Mason, T. G., Dhopple, A. and Wirtz, D. 1998. Linear Viscoelastic Moduli of Concentrated DNA Solutions. Macromolecules 31: 3600-3606.

37. Mason, T. G., 2000. Estimating the viscoelastic moduli of complex

fluid using generalized Stokes-Einstein equation. Rheol. Acta 39: 371-378.

38. Mason, T. G., Ganesan, K., van Zanten, J. H., Wirtz, D. and Kuo, S. C. 1997. Particle Tracking Microrheology of Complex Fluids. Phys. Rev. Lett 79: 3282-3285.

Chapter 2

Methodology

2.1 Preparation of plasmid DNA pHSG298

Both deuterated and hydrogenated plasmid DNA was prepared from Escherichia coli. BL21 bacteria were transformed with pHSG298 (2675bp). The bacterial pellets were harvested and lysed with an alkaline solution. The supernatant was further purified with an AKTA explorer chromatography system. Finally, the plasmid DNA was characterized by gel electrophoresis.

2.1.1 Isolation of deuterated DNA

The cell paste for the isolation of perdeuterated pHSG298 plasmid (2675 bp) was prepared at the ILL-EMBL Deuteration Laboratory, Grenoble. Cells were grown in deuterated minimal medium (1, 2, 3, 4, 5) containing 40 mg/L kanamycin. For preparation of fully deuterated medium, mineral salts were dried in a rotary evaporator (Heidolph) at 60 ^{o}C and labile protons were exchanged for deuterons by dissolving in a minimal volume of D_2O and re-dried. Perdeuterated d_8-glycerol (Euriso-top, France) was used as a carbon

source. A pre-culture of 150mL adapted cells were used to inoculate 1.3 L deuterated minimal medium in a 3 L fermenter. During the batch and fed-batch phases, the pH was adjusted to 6.9 by additional NaOD and the temperature to 30 ^{o}C. The gas-flow rate of sterile filtered air was 0.5 L per minute. Stirring was adjusted to ensure a dissolved oxygen tension (DOT) of 30%. The fed-batch phase was initiated when the optical density at 600 nm reached a value of 4. D_8-glycerol was added to the culture to keep the growth rate stable during fermentation. When OD_{600} reached a value of 15, cells were harvested and stored at 193 K. From 2 fermenter runs, 92 g of deuterated cell paste was obtained. 45 g of the paste was used for the extraction of plasmid in the predeuterated form.

2.1.2 Isolation of hydrogenated DNA

Hydrogenated pHSG298 plasmid (2675 bp) was prepared from Escherichia coli. A colony of BL21-pHSG298 was transformed and grown on a Luria Broth plate with kanamycim (25 mg/L). A single colony was taken to grow a starter culture in Luria Broth medium containing kanamycim at 37 ℃ for eight hours. The starter culture was then diluted 1000 times into Luria Broth medium containing kanamycim and grown at 37 ℃ for 12–16 h with vigorous shaking (280 rpm, OD600 reached 1.8 for each batch). The bacterial

cells were harvested by centrifugation at 6000 x g for 15 min at 4 ℃. The cell pellet was weighed and 60 g of cell paste was taken for the extraction of plasmid in the hydrogenated form.

The bacterial pellets were suspended in 0.5L of 50mM Tris-HCl buffer, pH 7.5, 10mM EDTA and subsequently lysed with 0.5L of an alkaline solution (0.2M NaOH, 1% SDS) at room temperature. The pH of the mixture of cell suspension and the alkaline solution was kept below 12.5. Bacterial genomic DNA, cell debris, and proteins were precipitated by additional 0.5L of 3M potassium acetate, pH 5.5, pre-chilled at 4 ^{o}C. The supernatant was collected after centrifugation at 20,000 x g for 30 minutes at 4 ^{o}C.

2.1.3 Purification by chromatography

The supernatant was first concentrated using the quickstand. Then the concentrated supernatant was pumped through a Sepharose 6 fast flow column (XK 50/30) equilibrated with **buffer A**: 2M $(NH_4)SO_4$, 10mM EDTA, and 100mM Tris-HCl, pH 7.0 with an AKTA explorer chromatography system (GE Life Sciences, columns and chromatography media were also purchased from GE). This gel filtration chromatography results in the removal of RNA and buffer exchange, as shown in Fig. 2.1.

The plasmid was purified by thiophilic interaction chromatography using a

column packed with PlasmidSelect as shown in Fig.2.2. The column was equilibrated with the above mentioned buffer A and eluted with a gradient to 0.4 M NaCl, 2M $(NH_4)SO_4$, 10mM EDTA, and 100mM Tris-HCl, pH 7.0 (6).

Finally, the sample was concentrated and endotoxins were removed by capturing the plasmid on a Source 30Q ion exchange column as shown in Fig.2.3. The plasmid was eluted in a gradient to 0.6 M NaCl. The ratio of the optical absorbencies A (260nm)/A (280nm) = 1.82 indicates that the material is free of protein. After precipitation with isopropanol, the DNA pellet was gently dried for a short period and dissolved in TE buffer (10 mM Tris, 1 mM EDTA, pH 8.0) and stored at 4 ^{o}C.

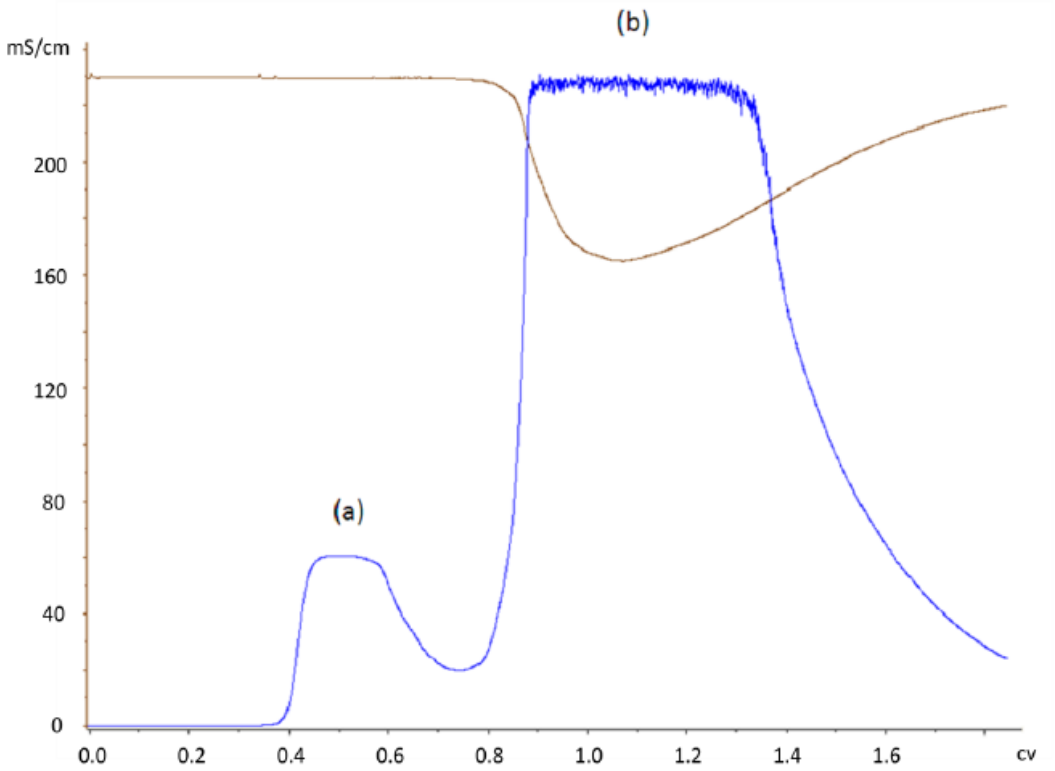

Fig.2.1 Conductivity versus column volume CV for the first Sepharose 6 gel filtration step. The brown line represents conductivity. The blue line represents the intensity of UV absorbance at 260 nm. Fraction (a) is DNA of lysate after pumping through Sepharose 6 fast flow column (XK 50/30). Fraction (b) is RNA of lysate after pumping through Sepharose 6 fast flow column (XK 50/30).

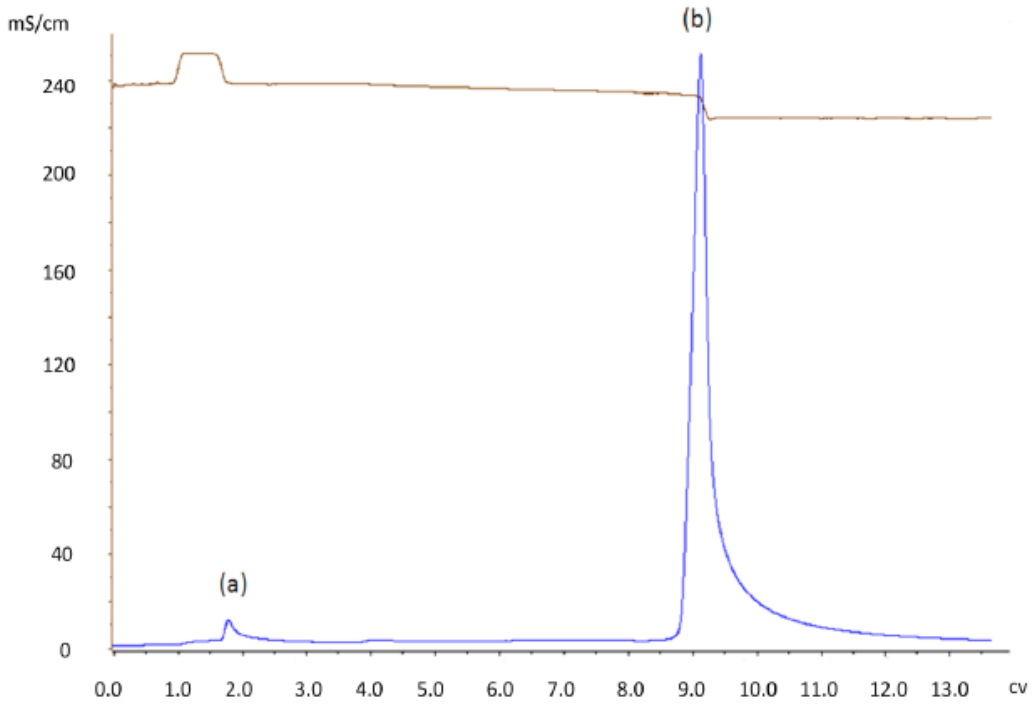

Fig.2.2 Conductivity versus column volume CV pertaining to the Plamid Select thiophilic interaction chromatography step. The brown line represents conductivity. The blue line represents the intensity of UV absorbance at 260 nm. Fraction (a) is open circular DNA of fraction (a) in Fig.2.1 after pumping through Plasmid-Select column. Peak (b) is supercoiled DNA of fraction (a) in Fig.2.1 after pumping through Plasmid-Select column.

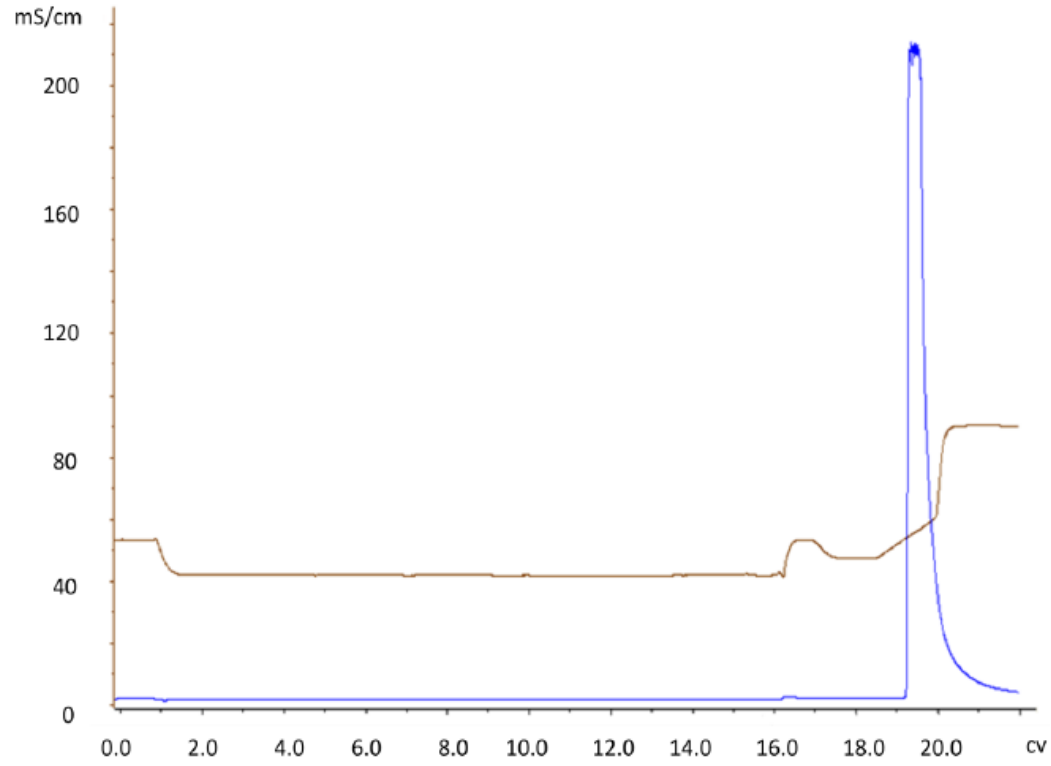

Fig.2.3 Conductivity versus column volume CV pertaining to the Source 30Q ion exchange step. The dash line represents conductivity. The solid line represents the intensity of UV absorbance at 260 nm. After pumping through Source 30Q column DNA was concentrated and endotoxin was removed.

2.2 Plasmid characterization

The integrity of the plasmid in both perdeuterated and hydrogenated forms, DNA^H and DNA^D, respectively, was checked with 1% agarose gel electrophoresis in TAE buffer (40mM Tris-acetate, 1mM EDTA, PH 8.3) at 70 V for 2 hours (7), as shown in Fig. 2.4. The linking number deficit and percentages of open circular and linear plasmids were determined by 1.4% agarose gel electrophoresis in TPE buffer (90mM Tris-phosphate, 1mM EDTA, PH 8.3) with optimized concentration of chloroquine at 50 V for 36 hours (8). Ethidium bromide was used to stain DNA after the gel electrophoresis running. The concentration of ethidium bromide used here is 1ug/ml.

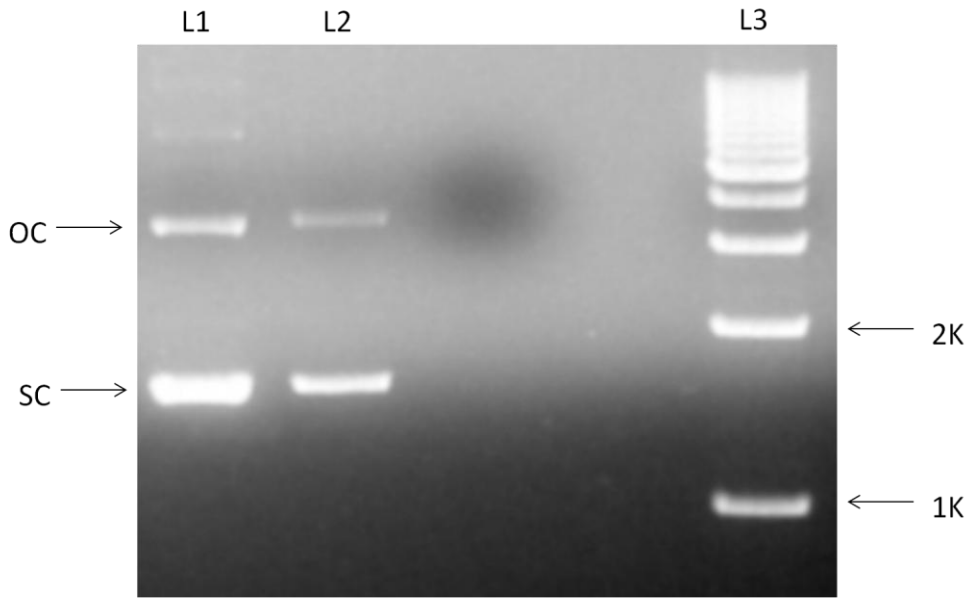

Fig.2.4 1% agarose gel electrophoresis in TAE buffer (40mM Tris-acetate, 1mM EDTA, PH 8.3) at 70 V for 2 hours. L1 and L2 are perdeuterated DNA. L3 is DNA ladder. The open circular and supercoiled DNA are indicated by OC and SC, respectively.

2.2.1 Superhelical density determination

Gaussian-type distributions of DNA bands are observed in circular DNA closed by ligase or by DNA-relaxing enzyme in the absence of EtdBr and are the result of thermal fluctuation in the DNA helix which leads to rotation of the two strands around the strand opposite the nicks (9, 10).

Because chloroquine (used as an unwinding ligand) causes a decrease in twist of the DNA double helix without changing the linking number, it increases the writhe (11, 12). Consequently, DNA molecules relaxed under incubation conditions become positively supercoiled, and highly negatively supercoiled DNA molecules become more relaxed. In the presence of chloroquine, the electrophoretic mobility of relaxed DNA molecules is increased, and, conversely, the mobility of negatively supercoiled DNA molecules is decreased.

To determine the superhelical density, the resolution of the topoisomers was manipulated by using various concentrations of chloroquine from 1 to 120 mg/L. Optimal separation of the topoisomers was observed at chloroquine phosphate concentrations of 3 mg/L and 80 mg/L, as shown in Fig. 2.5. At chloroquine

concentration of 3 mg/L, all molecules were negatively supercoiled. While at chloroquine concentration of 80 mg/L, all molecules were positively supercoiled.

The position of the band pertaining to $\Delta Lk = 0$ was determined by relaxation of the plasmid DNA^H with Topoisomerase II, Alpha (purchased from USB Corporation). Since Topoisomerase II cut one double strand of supercoiled DNA and let the other double strand pass through, fully relaxed supercoiled DNA has a linking number deficit of 0 and ± 1. Even linking number deficit relaxes to 0, whereas odd linking number deficit relaxes to either +1 or -1. 1.4% agarose gel electrophoresis of relaxed DNA was shown in Fig. 2.6 and Fig. 2.7. Relaxed DNA ($\Delta Lk = 0$) moves slowest, whereas $\Delta Lk = +1$ or $\Delta Lk = -1$ migrates a little faster at the same speed. When relaxed DNA^H was incubated in adequate chloroquine (80 mg/L), all relaxed molecules became more positively supercoiled than initially negatively supercoiled DNA. Hence the electrophoretic mobility of relaxed DNA^H molecules was the fastest (see Fig. 2.8 Lane 1). The superhelical densities of the hydrogenated and perdeuterated plasmids are similar, as shown in Fig. 2.8.

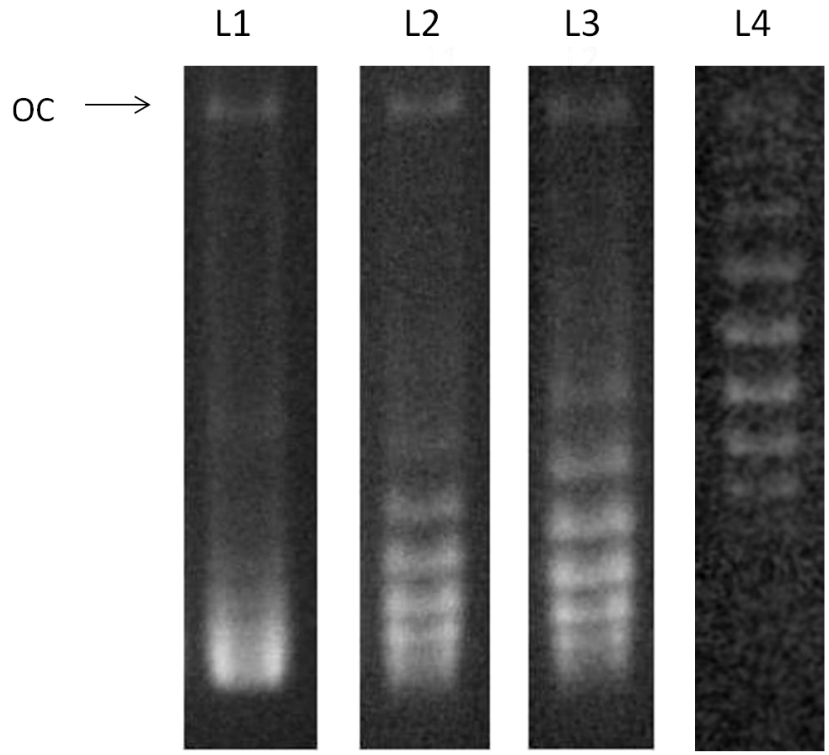

Fig.2.5 1.4% agarose gel electrophoresis in TPE buffer (90mM Tris-phosphate, 1mM EDTA, PH 8.3) at 50 V for 36 hours. The lanes are: DNA^D with cloroquine concentration of 1 mg/L (L1), DNA^D with cloroquine concentration of 3 mg/L (L2), DNA^D with cloroquine concentration of 5 mg/L (L3), DNA^D with cloroquine concentration of 80 mg/L (L2).

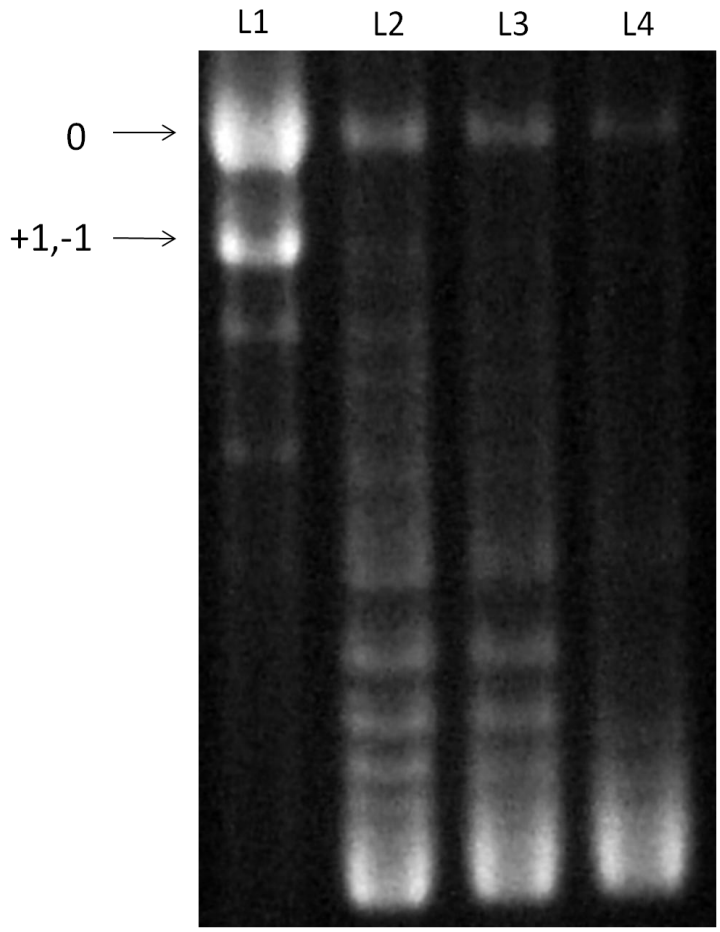

Fig. 2.6 Gel electrophoresis with 1 mg/L chloroquine phosphate. The lanes are: relaxed DNA^H (L1), DNA^H (L2), a 1:1 mixture of DNA^H and DNA^D (L3) and DNA^D (L4). The relaxed $\Delta Lk = 0$ and relaxed $\Delta Lk = +1$ or $\Delta Lk = -1$ states are indicated by 0 and +1, -1 respectively.

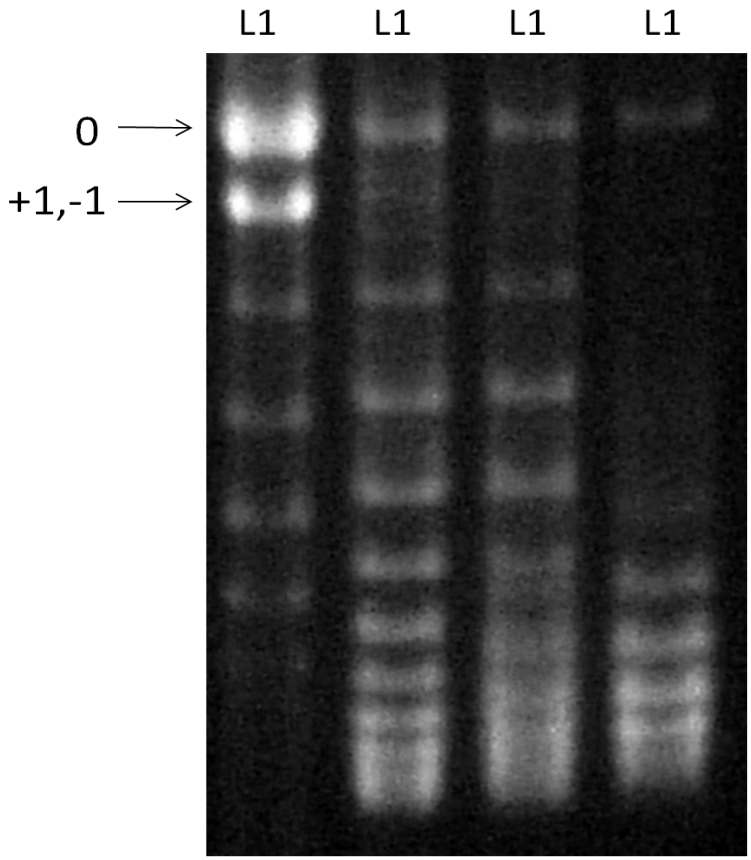

Fig. 2.7 Gel electrophoresis with 3 mg/L chloroquine phosphate. The lanes are: relaxed DNA^H (L1), DNA^H (L2), a 1:1 mixture of DNA^H and DNA^D (L3) and DNA^D (L4). The relaxed ($\Delta Lk = 0$) and relaxed ($\Delta Lk = +1$ or $\Delta Lk = -1$) states are indicated by 0 and +1, -1 respectively. The most abundant topoisomer has $\Delta Lk = -9 \pm 1$ (superhelical density $\sigma = 0.035$).

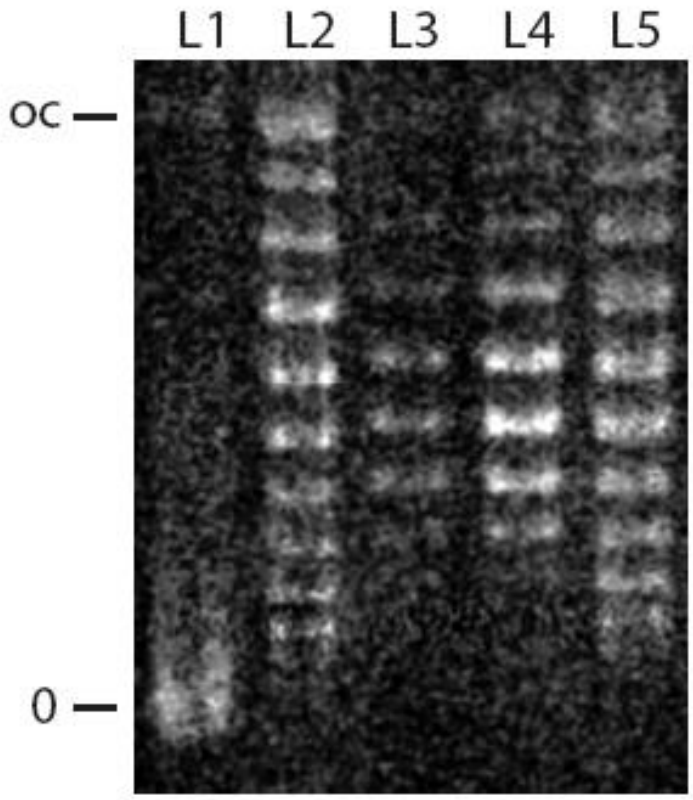

Fig. 2.8 Gel electrophoresis with 80 mg/L chloroquine phosphate. The lanes are: relaxed DNA^H (L1), DNA^H (L2), DNA^D (L3 and L4), and a 1:1 mixture of DNA^H and DNA^D (L5). The open circular and relaxed ($\Delta Lk = 0$) states are indicated by oc and 0, respectively. The most abundant topoisomer has $\Delta Lk = -9 \pm 1$ (superhelical density $\sigma = 0.035$).

2.3 Small angle neutron scattering

2.3.1 Background

Nowadays, there are several techniques which can be used to study the structure of DNA. The most important method, at least from a historical point of view, has been the analysis of DNA structure by X-ray diffraction. This is the tool which was used to discover the basic double-helical form of DNA in 1953 (17). By the development of cryo-electron and atomic force microscopy, DNA can be visualized (18, 19, 20, 21, 22). These direct techniques can also be used to determine the structures of DNA. One can be confident that these imaging results correspond to physical reality. However, it is often difficult to prepare indeed a sample for electron microscopy or a suitable crystal for X-ray scattering of a biologically interesting substance. To access three dimensional conformation properties of DNA, small angle scattering experiment is the best way (23, 24, 25). In structural studies neutron diffraction and neutron small angle scattering cover the same ranges of special resolution as X-ray diffraction and small angle scattering. The major difference between the techniques lies in the interaction between the probing radiation and the sample. X-ray are scattered by electrons, neutrons are scattered by nuclei. The strength of neutron-nuclear interaction is characterized by a property called ‘scattering

length', which is not a function of atomic number. The observation that hydrogen and deuterium differ markedly in the values of their neutron scattering length is of fundamental importance. Deuterium labeling is much less intrusive than labeling with heavy metals (as is done for X-ray investigations) so that labeled molecules (for example, DNA) can be studied in a neutron experiment surrounded by other molecules almost in their 'natural state'. In biological systems hydrogen can be exchanged with deuterium. This makes small angle neutron scattering particularly useful for the biological sciences.

In a SANS experiment a beam of neutrons passes through a pinhole, then is directed at a sample and finally reaches the detector. A sample can be an aqueous solution, a solid, a powder, or a crystal. Investigated by neutron scattering, information about the sample is converted into changes in wave vector and energy of the neutrons. The detector records the scattering profile, *i.e.* the neutron intensity as a function of the scattering angle. The scattering profile gives information about the size, shape and orientation of the structures of the sample. The scattering angle is generally small, less than 10^{o}, in order to obtain information about structures at large length scales, from 0.1 to 100 nm. These length scales are larger than those probed by conventional diffraction techniques.

In neutron scattering, when an object is illuminated by a monochromatic plane wave with wavevector $k_i = 2\pi/\lambda$, the nuclei scatterers within the object and which are interacting with the incident radiation become sources of spherical waves. Only elastic scattering is considered, *i.e*. scattering without energy transfer, so that the modulus of the scattered wave k_f is equal to the modulus of k_i.

Neutrons interact with the nuclear potential and with the spin of the nuclei. The neutron scattering length consists of two terms $f_n = f_p + f_s$. The last term bears structural information only if the neutron spins in the incident beam and the nuclear spins in the object are polarized, otherwise the spin scattering yields only a flat incoherent background. However, f_p does not increase with the atomic number, but is sensitive to the isotope.

2.3.2 Interpretation of scattering intensity

It is not possible to proceed much further in the discussion of neutron scattering without looking at the processes in which information about the sample is converted into changes in wavevector and energy of the neutrons. The scattering intensity is determined by the interference of scattered radiation from assemblies of atoms. For simplification, only the interference of scattered radiation from two atoms of two layers with scattering length b_1 and b_2 is

considered, respectively. Fig.2.11 and Fig.2.12 illustrate the scattering process.

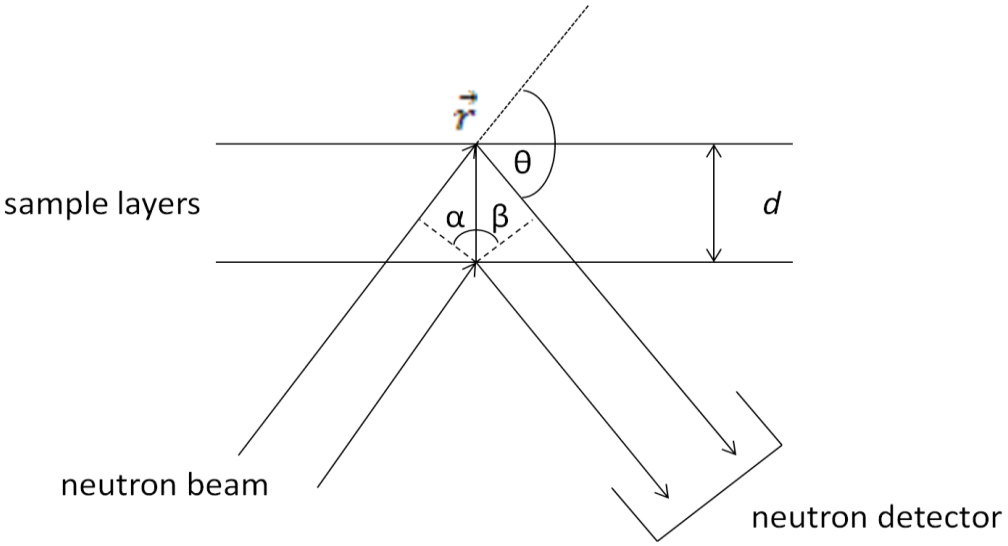

Fig. 2.9 Diffraction of neutrons by two layers.

An incident radiation with wavevector $k_i = 2\pi/\lambda$ is scattered by two atoms with a special separation $\vec{r}$. The scattering intensity at scattering angle θ is given by

$$I = \left|b_1 + b_2 e^{ik\Delta L}\right|^2 \tag{2.1}$$

While optical path difference ΔL between the scattering waves from the two points separated by $\vec{r}$ is given by

$$\Delta L = r\sin\alpha + r\sin\beta = \vec{r}\cdot(2\sin(\theta/2)\vec{q}_0) \tag{2.2}$$

, with $\vec{q}_0$ the unit vector of $\vec{k}_i - \vec{k}_f = \vec{q}$

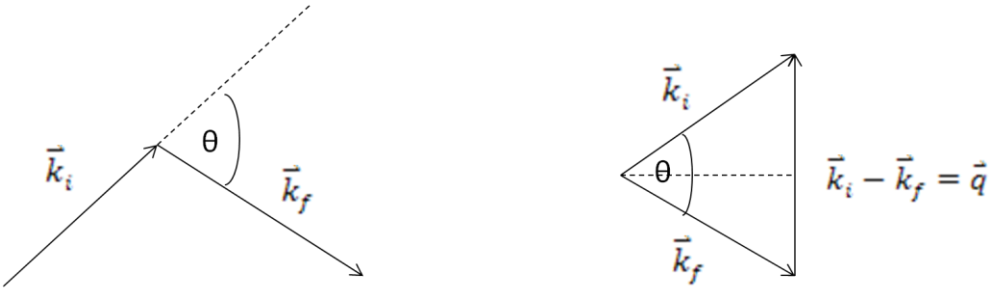

Fig.2.10 Relationship between wavevector and momentum transfer for elasticscattering.

The phase difference between the scattering waves from the two points separated by $\vec{r}$ is given by

$$\Delta\phi = k\Delta L = \vec{r} \cdot (4\pi sin(\theta/2)/\lambda \times \vec{q}_0) \quad (2.3)$$

After introducing the momentum transfer

$$\vec{q} = 4\pi sin(\theta/2)/\lambda \times \vec{q}_0 \quad (2.4)$$

, eq. (2.1) can be rewritten as

$$I = \left|b_1 + b_2 e^{i\vec{q}\cdot\vec{r}}\right|^2 \quad (2.5)$$

Now we consider a more realistic situation. For assemblies of atoms, we define the scattering length density distribution $\rho(\vec{r})$, which equals to total scattering length of atoms per unit volume. Then the scattering intensity becomes

$$I = \left|\int d\vec{r}\rho(\vec{r})\, e^{i\vec{q}\cdot\vec{r}}\right|^2 \quad (2.6)$$

The scattering is the square of the scattering amplitude A(q), which is the Fourier transform of the spatial distribution of the scattering length.

The SAS experiments on macromolecules dispersed in solutions involve the scattering contributions from both macromolecules and solvent (water). The structural features of the solvent are often smaller than the length scale of interest and thus we can assume that the solvent is featureless with a constant

scattering density ρ_s. The solvent contributes as a uniform background to the scattering intensity and, hence, we can define the excess scattering length density of the solute with respect to the solvent, $\Delta\rho(r) = \rho(r) - \rho_s$. Then, the scattering amplitude is the Fourier transform of $\Delta\rho(r)$. The average excess density of the particle $\Delta\rho(r) = <\Delta\rho(r)>$, which is usually called the contrast, is an important characteristic of the sample. With a larger contrast the scattering intensities are more intense and statistically better results can be obtained. For neutron scattering, the scattering length contrast can be adjusted by the ratio of H_2O/D_2O, due to the large difference of scattering length between H and D.

In a scattering experiment one cannot directly measure the scattering amplitude A(q), but only the scattering intensity $I(q) = |A(q)|^2$. The intensity is proportional to the number of photons or neutrons scattered in the given direction. The detector only records a range of scattering angles, usually from 0.1^o to 10^o. In addition, the orientations of the solutes (macromolecules) are often random, sometimes partially ordered, and then the recorded scattering intensity is spherically averaged. These features of SAS have two consequences. First, the scattering intensity I(q) is usually a rapidly decaying function of momentum transfer q and only low resolution patterns ($d>>\lambda$) are available. Second, the detailed structure of the solute cannot be calculated directly from the scattering intensity I(q). The usual way of qualitative

interpretation of SAS data is by assumption of a solute structure and density distribution, deriving I(q) from ρ(r) and then comparing the theoretical prediction with experimental data. The comparison examines the validity of the assumed structure and determines the values of possible fitting parameters.

In this thesis, the effect of crowding on the conformation of inter-wound DNA strands is studied through small angle neutron scattering measurements. The distance between two opposing duplexes in supercoiled DNA is determined with the help of neutron scattering in the condition of zero and full average contrast.

Reference

1. Forsyth, V. T., Myles, D., Timmins, P. A. and Haertlein, M. 2001. Possibilities for the exploitation of biological deuteration in neutron scattering, in J. Dianoux (Ed) Opportunities for Neutron Scattering in the 3rd Millennium. Institut Laue Langevin publication pp: 4754.
2. Laux, V., Callow, P., Svergun, D. I., Timmins, P. A., Forsyth, V. T. and Haertlein, M. 2008. Selective deuteration of tryptophan and methionine residues in maltose binding protein: a model system for neutron scattering. Eur Biophys J 37: 815-822.

3. Artero, J. B., Haertlein, M., McSweeney, S., Timmins, P. A. 2005. A comparison of refined Xray structures of hydrogenated and perdeuterated rat Ecrystallin in H2O and D2O. Acta Cryst D 61: 1541-1549.

4. Di Costanzo, L., Moulin, M., Haertlein, M., Meilleur, F. and Christianson, D. W. 2007. Expression, purification, assay, and crystal structure of perdeuterated human arginase I. Arch Biochem Biophys 465: 82-89.

5. Wood K, Frölich, A., Paciaroni, A., Moulin, M., Härtlein, M., Zaccai, G., Tobias, D. J. and Weik, M. 2008. Coincidence of dynamical transitions in a soluble protein and its hydration water: Direct measurements by neutron scattering and MD simulations. J Am Chem Soc 130: 4586-4587.

6. Sandberg, L. M., Bjurling, A., Busson, P., Vasi, J., Lemmens, R. 2004. Thiophilic interaction chromatography for supercoiled plasmid DNA purification. J. Biotechnology 109: 193-199.

7. Backendorf, C., Olsthoorn, R., van de Putte, P. 1989. Superhelical stress restrained in plasmid DNA during repair synthesis initiated by the UvrA, Bprotein and Cproteins in vitro. Nucleic Acids Res 17: 10337-10351.

8. Shure, M., Pulleyblank, D. E. and Vinograd, J. 1977. The problems of eukaryotic and prokaryotic DNA packaging and in vivo conformation posed by superhelix density heterogeneity. Nucleic Acids Res 4: 1183-1205.

9. Westerhoff, H. V., O'Dea, M. H., Maxwell, A. and Gellert, M. 1988. DNA supercoiling by DNA gyrase. A static head analysis. Cell Biophys 12: 157-181.

10. Fisher, L.M., 1981. DNA supercoiling by DNA gyrase. Nature 294: 607-608.

11. Keller, W., 1975. Determination of the number of superhelical turns in simian virus 40 DNA by gel electrophoresis. Proc Natl Acad Sci U S A, 72: 4876-4880.

12. Shure, M. and Vinograd, J. 1976. The number of superhelical turns in native virion SV40 DNA and minicol DNA determined by the band counting method. Cell 8: 215-226.

13. Yamada, H., Yoshida, T., Tanaka, K., Sasakawa, C., Mizuno, T. 1991. Molecular analysis of the Escherichia coli hns gene encoding a DNA-binding protein, which preferentially recognizes curved DNA sequences. Mol Gen Genet 230: 332-336.

14. Tanaka, K., Yamada, H., Yoshida, T. and Mizuno, T. 1991.

Overproduction and rapid purification of the Escherichia coli histone-like protein, H-NS. Agric. Biol. Chem 55: 3139-3141.

15. Dame, R.T., Wyman, C. and Goosen, N. 2000. H-NS mediated compaction of DNA visualised by atomic force microscopy. Nucleic Acids Res 28: 3504-3510.

16. Dame, R. T., Noom, M. C. and Wuite, G. J. 2006. Bacterial chromatin organization by H-NS protein unravelled using dual DNA manipulation. Nature 444: 387-390.

17. Watson, J. D. and Crick, F. H. 1953. The structure of DNA. Cold Spring Harb Symp Quant Biol 18: 123-131.

18. Lyubchenko, Y. L. 2004. DNA structure and dynamics: an atomic force microscopy study. Cell Biochem Biophys 41: 75-98.

19. Limanskii, A. P. 2000. Visualization of the cruciform structure of superhelical DNA by use of atomic force microscopy. Biofizika 45: 1039-1043.

20. Bednar, J., Furrer, P., Katritch, V., Stasiak, A. Z., Dubochet, J. and Stasiak, A. 1995. Determination of DNA persistence length by cryo-electron microscopy. Separation of the static and dynamic contributions to the apparent persistence length of DNA. J Mol Biol 254: 579-594.

21. Lepault, J., Dubochet, J., Baschong, W. and Kellenberger, E. 1987. Organization of double-stranded DNA in bacteriophages: a study by cryo-electron microscopy of vitrified samples. EMBO J 6: 1507-1512.

22. Duda, R. L., Ross, P. D., Cheng, N., Firek, B. A., Hendrix, R. W., Conway, J. F. and Steven, A. C. 2009. Structure and energetics of encapsidated DNA in bacteriophage HK97 studied by scanning calorimetry and cryo-electron microscopy. J Mol Biol 391: 471-483.

23. Neylon, C. 2008. Small angle neutron and X-ray scattering in structural biology: recent examples from the literature. Eur Biophys J 37: 531-535.

24. Zhou, J., Gregurick, S. K., Krueger, S. and Schwarz, F. P. 2006. Conformational changes in single-strand DNA as a function of temperature by SANS. Biophys J 90: 544-551.

25. Heller, W. T. and Littrell, K. C. 2009. Small-angle neutron scattering for molecular biology: basics and instrumentation. Methods Mol Biol 544: 293-305.

Chapter 3

Viscoelasticity of entangled lambda DNA solutions

3.1 Introduction

The dynamical properties of DNA have an impact on many biological processes such as the transcription of the genome and the segregation of the intertwined sister chromatids during mitosis. At high concentration, DNA molecules become entangled and they form a temporary dynamic network. Entanglements are topological constraints resulting from the fact that the DNA molecules cannot cross through each other. As a result of these entanglements, concentrated solutions of DNA have a complex viscoelasticity. The motion of the DNA molecules is strongly hindered by the presence of the neighboring DNA molecules and the relaxation times may become very long. Polymer dynamics under entangled conditions can be described by the reptation model, in which the polymer is thought to move in a snake-like fashion along the axial line (primitive path) of a tube formed by the entanglements (1). The reptation model gives specific scaling laws for the longest, global relaxation time, self-diffusion coefficient, high frequency limiting value of the elastic

storage modulus, and the zero shear limit of the viscosity of neutral polymers in the entangled regime. For a salted polyelectrolyte with screened electrostatic interactions the scaling laws are the same as for neutral polymers, albeit with different pre-factors related to an ionic strength dependent persistence length and excluded volume (2).

The viscoelastic properties of entangled DNA solutions have been reported before in the literature. Musti *et al*. reported the low shear viscosity and relaxation times of T2-DNA (164 kbp, contour length of 56 μm). It was shown that the reduced viscosity obeys the same scaling law as for synthetic linear polymers and that the entanglement concentration is 0.25 g of DNA/L. For solutions of 1 g of DNA/L the relaxation times become very long on the order of 1000 s (3). For λ-phage DNA (48.5 kbp, dye adjusted contour length of 22 μm) similar scaling behavior of the zero shear viscosity was observed, but the relaxation times are two orders of magnitude shorter because of the lower molecular weight (4). Smith *et al*. showed that the self-diffusion coefficient of λ-phage DNA follows the reptation prediction for concentrations exceeding 0.63 g/L (5). The viscous loss and the elastic storage moduli of calf-thymus DNA (13 kbp) through the entanglement concentration were reported by Mason *et al* (6). For concentrations exceeding the entanglement concentration, the loss modulus is crossed by the storage modulus at a crossover frequency ω_c and the storage modulus levels off at a limiting high frequency plateau value. A region of weak dependence of the steady state shear stress of

T4-DNA (166 kbp) on the shear rate has been reported by Jary *et al* (7). The concentration dependence of the lower boundary frequency scales as the reciprocal tube renewal or disengagement time, whereas the upper boundary corresponds with the Rouse relaxation time of the entire DNA molecule within the tube. Although these previous investigations are important in their own right, a comprehensive characterization of the viscoelasticity in terms of the viscous loss and elastic storage moduli of DNA solutions of rigorous monodispersity with increasing concentration through the entanglement transition is lacking.

Particle tracking microrheology is employed here, which requires minute samples of no more than 15 μL for each sample (8). Hence, this methodological approach is particularly promising for the investigation of biological samples of which only small quantities are available. In this chapter, elastic storage and viscous loss moduli of λ-phage DNA (48.5 kbp, contour length of 16.3 μm) dispersed in 10 mM Tris/EDTA buffer are reported. The effect of DNA concentration through the critical entanglement concentration on the viscoelastic properties is systematically explored. The number of entanglements per chain is derived from the limiting high frequency plateau value of the elastic storage modulus. The longest, global, relaxation time is obtained from the crossover frequency ω_c for entangled solutions as well as from the ratio of the low shear viscosity increment and the high frequency elasticity modulus for all samples. Finally, the results for the viscosity

increment, number of entanglements per chain, and the longest relaxation time are compared with the relevant scaling laws for reptation dynamics of salted polyelectrolytes.

3.2 Particle tracking microrheology

The viscoelastic properties of the DNA solution are probed by monitoring the one-dimensional mean square displacement $\langle \Delta x^2(t) \rangle$ over a time t of an embedded colloidal and spherical bead of radius a. The one-sided, complex Fourier transform of the mean square displacement

$$\langle \Delta \tilde{x}^2(\omega) \rangle = \int_0^\infty dt \exp(-i\omega t) \langle \Delta x^2(t) \rangle \quad . \qquad [1]$$

, is related to the elastic storage $G'(w)$ and viscous loss $G''(w)$ moduli of the medium through the generalized Stokes-Einstein equation

$$G'(\omega) + iG''^{(\omega)} = \frac{k_B T}{3\pi a i \omega \langle \Delta \tilde{x}^2(\omega) \rangle} \quad . \qquad [2]$$

with $k_B T$ being the thermal energy (8). The generalized Stokes-Einstein equation is valid under the same conditions as the Stokes equation for the friction experienced by the bead, *i.e.* no slip boundary conditions on a sphere in an isotropic, incompressible fluid and neglect of the sphere's inertia. Furthermore, it is assumed that the Stokes drag for a viscous fluid may be extended to viscoelastic materials over all frequencies and that the fluid

surrounding the bead can be treated as a continuum. The latter condition requires that the structures of the fluid which give rise to the viscoelastic properties (*e.g.*, the mesh size in a semi-dilute polymer solution) are much smaller than the size of the bead. In the range of concentrations from 0.1 g/L to 0.8 g/L, the mesh size is typically less than 100 nm and on the order of the DNA persistence length (the bead size is in the range of 1.0 μm to 3.2 μm (9). The effect of depletion in DNA concentration in the interfacial layer surrounding the bead will be considered below. The formalism also requires no hydrodynamic interactions among the beads, so that individual beads need to be separated over sufficiently large distances.

In order to evaluate the viscoelastic moduli, the one sided Fourier transform of the mean square displacement can be algebraically estimated by expanding $\ln\left\langle \Delta x^2(t)\right\rangle$ around the value of the logarithm of the mean square displacement $\ln\left\langle \Delta x^2(t')\right\rangle$ at $t' = \omega^{-1}$, *i.e.* $\ln\left\langle \Delta x^2(\omega^{-1})\right\rangle$ in powers of $\ln \omega t$ (10). Since in the double logarithmic representation the mean square displacement shows some curvature (as shown in Fig. 1), we have carried the expansion up to and including third order

$$\left\langle \Delta x^2(t)\right\rangle \approx \left\langle \Delta x^2(w^{-1})\right\rangle (wt)^{\alpha+\beta\ln\omega t+\gamma\ln^2\omega t}. \qquad [3]$$

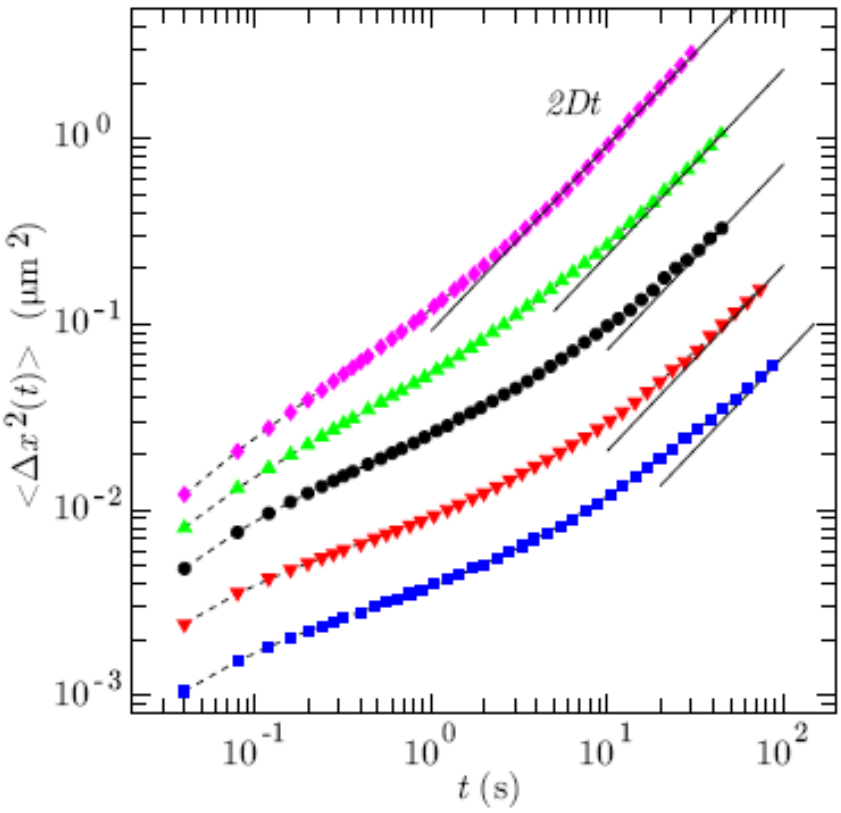

Fig. 3.1 Mean square displacement $\langle \Delta x^2(t) \rangle$ versus time t. The DNA concentrations are 0.8 (■), 0.6 (▼), 0.4 (●), 0.3 (▲), and 0.2 (♦) g of DNA per L. The solid lines represent diffusion behavior $\langle \Delta x^2(t) \rangle = 2Dt$ with D the diffusion coefficient of the colloidal bead for long times. The dashed lines represent fourth order polynomial fits.

The frequency dependent coefficients are defined by the first, second, and third order derivatives

$$\alpha = \left.\frac{\partial \ln\left\langle \Delta x^2(t')\right\rangle}{\partial \ln t'}\right|_{t'=\omega^{-1}},$$

$$\beta = \left.\frac{1}{2}\frac{\partial^2 \ln\left\langle \Delta x^2(t')\right\rangle}{\partial \ln t'^2}\right|_{t'=\omega^{-1}}, \qquad [4]$$

$$\gamma = \left.\frac{1}{6}\frac{\partial^3 \ln\left\langle \Delta x^2(t')\right\rangle}{\partial \ln t'^3}\right|_{t'=\omega^{-1}}.$$

In the case of diffusive behavior $\alpha = 1$, because $\left\langle \Delta x^2(t)\right\rangle = 2Dt$ with D being the diffusion coefficient of the bead. For fully elastic response with a constant mean square displacement, one obviously has $\alpha = 0$, so that $0 \le \alpha \le 1$. The integral transform Eq. [1] with the power series expansion Eq. [3] for $\left\langle \Delta x^2(t)\right\rangle$ cannot be solved in closed analytical form. However, since β and γ are small with respect to the leading term α, Eq. [3] can be expanded in powers of β and γ:

$$\left\langle \Delta x^2(t)\right\rangle \approx \left\langle \Delta x^2(\omega^{-1})\right\rangle (\omega t)^{\alpha}(1 + \beta \ln^2 \omega t + \gamma \ln^3 \omega t + \beta^2/2 \ln^4 \omega t + \beta\gamma \ln^5 \omega t + \gamma^2/2 \ln^6 \omega t + \cdots) \qquad [5]$$

We will retain the terms up to and including second order in β and γ. The one-sided Fourier transform of the mean square displacement Eq. [1] can now be evaluated in analytical form by integration of Eq. [5] term by term (higher

order terms can also be integrated if desired). The complex viscoelastic modulus follows then from Eq. [2] and takes the form

$$G(w) = \frac{k_B T(Cos(\alpha\pi/2) + i\,Sin(\alpha\pi/2))}{3\pi a\left\langle \Delta x^2(\omega^{-1})\right\rangle \Gamma(1+\alpha)(1+c_1+c_2+c_3+c_4+c_5+\cdots)}. \qquad [6]$$

where Γ denotes the gamma function and the (complex) coefficients c_1 through c_5 are given in bellowing table. The latter coefficients are related to β and γ, which describe the deviation from linearity of the mean square displacement in the double logarithmic representation. To lowest order, it is sufficient to include c_1, which is proportional to the second order derivative β. For the analysis of data which show a strong deviation from linearity, it is necessary to include the higher order coefficients. Although the corresponding expressions are quite lengthy, they can be implemented without computational difficulties.

Table 3.1: Coefficients in the expression of the viscoelastic moduli pertaining to the curvature in the mean square displacement up to and including second order in β and γ. ψ^{n} denotes the n^{th} order polygamma function.

$$c_1 = \beta/4\left(4\psi^{(1)}(\alpha+1) - \left(2i\psi^{(0)}(\alpha+1)+\pi\right)^2\right) \quad [7]$$

$$c_2 = \gamma/8\left(i\left(2i\psi^{(0)}(\alpha+1)+\pi\right)^3 + 12\left(-i\pi + 2\psi^{(0)}(\alpha+1)\right)\psi^{(1)}(\alpha+1) + 8\psi^{(2)}(\alpha+1)\right) \quad [8]$$

$$\begin{aligned} c_3 = \beta^2/32\big(&8\left(2\psi^{(0)}(\alpha+1)^4 - 4i\pi\psi^{(0)}(\alpha+1)^3 - 3\left(\pi^2 - 4\psi^{(1)}(\alpha+1)\right)\psi^{(0)}(\alpha+1)^2 + \right.\\ &\left(i\pi\left(\pi^2 - 12\psi^{(1)}(\alpha+1)\right) + 8\psi^{(2)}(\alpha+1)\right)\psi^{(0)}(\alpha+1) + 6\psi^{(1)}(\alpha+1)^2 - \\ &\left.3\pi^2\psi^{(1)}(\alpha+1) - 4i\pi\psi^{(2)}(\alpha+1)\right) + \pi^4 + 16\psi^{(3)}(\alpha+1)\big) \end{aligned} \quad [9]$$

$$\begin{aligned} c_4 = \beta\gamma/32\big(&32\psi^{(0)}(\alpha+1)^5 - 80i\pi\psi^{(0)}(\alpha+1)^4 - 80\left(\pi^2 - 4\psi^{(1)}(\alpha+1)\right)\psi^{(0)}(\alpha+1)^3 + \\ &40i\left(-12\pi\psi^{(1)}(\alpha+1) + \pi^3 - 8i\psi^{(2)}(\alpha+1)\right)\psi^{(0)}(\alpha+1)^2 + \\ &10\left(-8\left(3\psi^{(1)}(\alpha+1)\left(\pi^2 - 2\psi^{(1)}(\alpha+1)\right) + 4i\pi\psi^{(2)}(\alpha+1)\right) + \pi^4 + \right.\\ &\left.16\psi^{(3)}(\alpha+1)\right)\psi^{(0)}(\alpha+1) - i\left(240\pi\psi^{(1)}(\alpha+1)^2 - \right.\\ &\left.40\left(\pi^3 - 8i\psi^{(2)}(\alpha+1)\right)\psi^{(1)}(\alpha+1) + \pi^5 + \right.\\ &\left.80\pi\left(\psi^{(3)}(\alpha+1) - i\pi\psi^{(2)}(\alpha+1)\right) + 32i\psi^{(4)}(\alpha+1)\right)\big) \end{aligned} \quad [10]$$

$$c_5 = \gamma^2/128\left(4\left(16\psi^{(0)}(\alpha+1)^6 - 48i\pi\psi^{(0)}(\alpha+1)^5 - 60\left(\pi^2 - 4\psi^{(1)}(\alpha+1)\right)\psi^{(0)}(\alpha+1)^4 + \right.\right.$$
$$40i\left(-12\pi\psi^{(1)}(\alpha+1) + \pi^3 - 8i\psi^{(2)}(\alpha+1)\right)\psi^{(0)}(\alpha+1)^3 +$$
$$15\left(-8\left(3\psi^{(1)}(\alpha+1)\left(\pi^2 - 2\psi^{(1)}(\alpha+1)\right) + 4i\pi\psi^{(2)}(\alpha+1)\right) + \right.$$
$$\left.\pi^4 + 16\psi^{(3)}(\alpha+1)\right)\psi^{(0)}(\alpha+1)^2 - 3i\left(240\pi\psi^{(1)}(\alpha+1)^2 - \right.$$
$$40\left(\pi^3 - 8i\psi^{(2)}(\alpha+1)\right)\psi^{(1)}(\alpha+1) + \pi^5 + 80\pi\left(\psi^{(3)}(\alpha+1) - \right.$$
$$\left.i\pi\psi^{(2)}(\alpha+1)\right) + 32i\psi^{(4)}(\alpha+1)\Big)\psi^{(0)}(\alpha+1) + 5\left(48\psi^{(1)}(\alpha+1)^3 - \right.$$
$$36\pi^2\psi^{(1)}(\alpha+1)^2 + 3\left(-32i\pi\psi^{(2)}(\alpha+1) + \pi^4 + 16\psi^{(3)}(\alpha+1)\right)\psi^{(1)}(\alpha+1) +$$
$$\left.4\left(8\psi^{(2)}(\alpha+1)^2 + 2i\pi^3\psi^{(2)}(\alpha+1) - 3\pi^2\psi^{(3)}(\alpha+1)\right)\right) -$$
$$\left.48i\pi\psi^{(4)}(\alpha+1)\right) - \pi^6 + 64\psi^{(5)}(\alpha+1)\Big)$$

[11]

3.3 Experimental section

3.3.1 sample preparation

Bacteria phage λ-DNA was purchased from New England Biolabs, Ipswich, MA and used without further purification. Single stranded DNA with a base pair sequence complementary to the λ-phage DNA overhang was purchased from Aldrich. As received from the manufacturer the λ-phage DNA stock solution has a concentration of 0.5 g of DNA/L. The solvent is TE buffer, which is composed of 10 mM Tris-HCl, pH 8.0, and 1 mM EDTA. Water was deionized and purified by a Millipore system and has a conductivity less than $1\times10^{-6}\ \Omega^{-1}cm^{-1}$. The DNA stock solution was concentrated to a concentration of about 1 g of DNA/L by freeze drying and subsequently extensively dialyzed in microdialyzers against TE buffer. The DNA concentration of the stock solution was determined by UV spectrometry. A series of samples with DNA concentrations in the range 0.2-0.8 g/L was subsequently prepared by dilution of the stock solution with TE buffer. The samples were spiked with polystyrene microspheres (Polysciences, Warrington, PA) of 0.99 ± 0.03 μm diameter with a final concentration of less than 0.1 wt %. For each particle tracking experiment, a droplet of solution was deposited on a microscopy slide and sealed with a coverslip separated by a 0.12 mm spacer. Sticky ends were

removed by heating the sample to 338 K for 10 minutes and subsequent cooling to ambient temperature as well as by the addition and hybridization of the complementary single stranded DNA, so that they have no significant effect on the viscoelastic properties.

3.3.2 Particle tracking

Particle tracking experiments were carried out at ambient temperature (296 K) with a Leica DM EP microscope equipped with a 50 times long working distance and 100 times oil immersion objectives. In order to minimize hydrodynamic interactions, care was taken that the imaged beads are at least 20 bead diameters (20 μm) apart. Furthermore, the height level of the focal plane was adjusted so that it is situated right between slide and coverslip with maximum separation. Video was collected with a charge coupled device (CCD) camera (JVC TK-C921EG) connected via an analog-to-digital video converter (Canopus, ADVC55) to a computer. For each sample, at least 10 movies with a total duration exceeding 100 minutes of at least 10 different beads were recorded with a rate of 25 frames per second and stored on hard disk. The video was analyzed with MATLAB (Natick, MA) using an AVI file reader and the particle trajectories were obtained with public domain tracking software (http://physics.georgetown.edu/matlab/). All further data analysis was done with home developed software scripts written in MATLAB code. The pixel

resolutions in the x and y directions were calibrated with the help of a metric ruler. Experimental setup was checked by measuring the diffusion of colloidal beads dispersed in concentrated solution of glycerol as well as by monitoring immobilized beads absorbed at a glass slide.

3.4 Results and discussion

3.4.1 Mean square displacement

From the bead trajectories, the probability distributions for displacements in the x and y directions were extracted for a range of displacement times t. The minimum displacement time $t = 40$ ms is determined by the frame rate of the video camera. The maximum time is in principle unbound. But in practice it is set by the rheological properties of the sample, because the particles eventually diffuse out of the field of view and/or they are subjected to long time coherent flow. For samples used in this chapter, a practical upper limit of the displacement time is about 100s. A Gaussian was fitted to both probability distributions by optimizing the mean square displacements. The mean square displacements in the two orthogonal directions were checked to be equal within experimental error, therefore the average value was reported. Some typical results are displayed in Fig. 1. For the sake of clarity, results pertaining to 0.7 and 0.5 g of DNA/l are not included. The latter results fall

perfectly between the marks set by the 0.8, 0.6 and 0.4 g of DNA/l solutions. Note that the symbol $\left\langle \Delta x^2(t) \right\rangle$ are used to stress that we are referring to the mean square displacement in one dimension; albeit the experimental results are obtained by statistically averaging the widths of the distributions obtained in the *x*- and *y*-directions (these widths are identical within experimental error because the fluid is isotropic).

In the double logarithmic representation and with increasing time, the mean square displacement of a dispersed colloidal bead first increases, after which it levels off to a certain extent depending on the DNA concentration, and eventually increases again. For very long times, diffusive behavior is recovered with $\left\langle \Delta x^2(t) \right\rangle$ proportional to the time t. The deviation from diffusive behavior for shorter times is typical of a viscoelastic, complex fluid. Due to temporary entanglements formed by the DNA molecules, the solution exhibits an elastic response at short times. As we will see shortly, the longest, global relaxation time of the λ-phage DNA molecules is on the order of a second. For longer times entanglements are relaxed, the molecules can move over their molecular dimensions, and the solution behaves as a viscous fluid. With increasing DNA concentration, the mean square displacement decreases and the range of times with a sub-diffusive scaling exponent less than one becomes wider. These phenomena are obviously related to changes in the viscoelasticity, which are more conveniently discussed in terms of the viscous loss and the elastic storage moduli to be presented below.

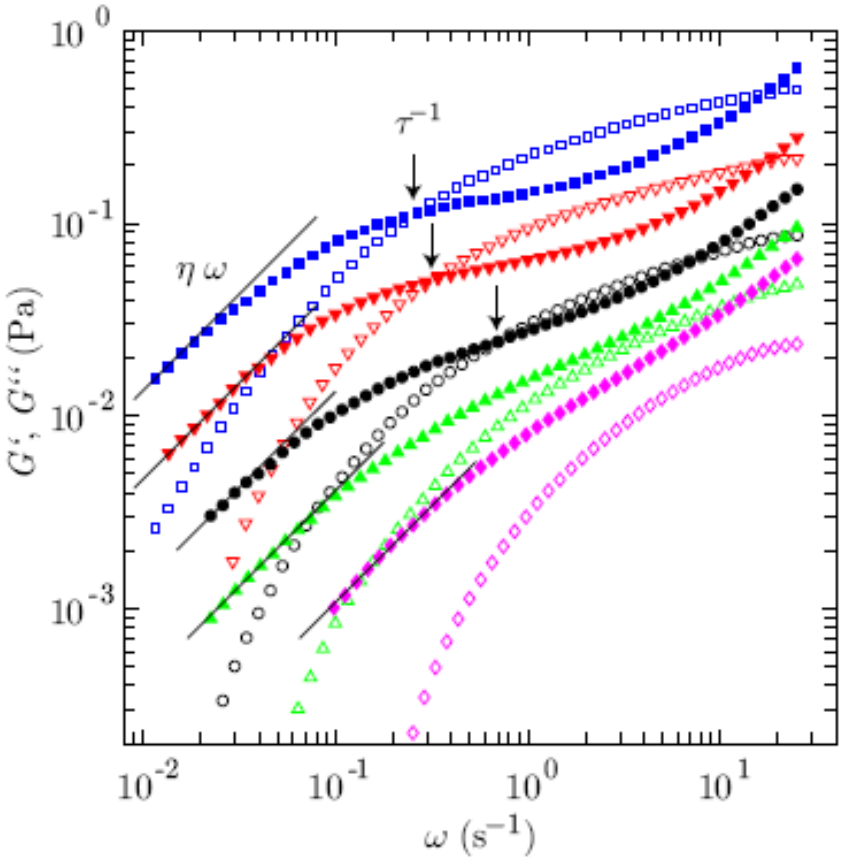

Fig. 3.2 Elastic storage G' (open symbols) and viscous loss G'' (closed symbols) versus frequency ω. The DNA concentrations are as in Fig. 1. The solid lines represent the low frequency limiting behavior $G'' = \eta\omega$ with the low shear viscosity η. The arrows denote the lowest crossover frequencies corresponding with the inverse relaxation times.

For a viscous fluid, the mean square displacement is given by Einstein's law $\left\langle \Delta x^2(t) \right\rangle = 2Dt$ with D being the diffusion coefficient. With the Stokes-Einstein equation $D = k_B T / 6\pi\eta a$, we can thus derive the low shear viscosity η of the DNA solution from the limiting long-time diffusive behavior of the mean square displacement. The measured viscosity increments $\Delta\eta = \eta - \eta_s$ with respect to the one of the solvent $\eta_s = 0.001$ Pa s are displayed Fig. 3.3. The viscosity increment increases by more than two orders of magnitude if the DNA concentration increases from 0.2 to 0.8 g/L. Furthermore, it follows a power law $\Delta\eta \simeq c^{3.93}$ pertaining to an entangled polyelectrolyte solution with screened electrostatics in an excess of simple salt with a Flory exponent $\nu = 0.588$ (2, 3).

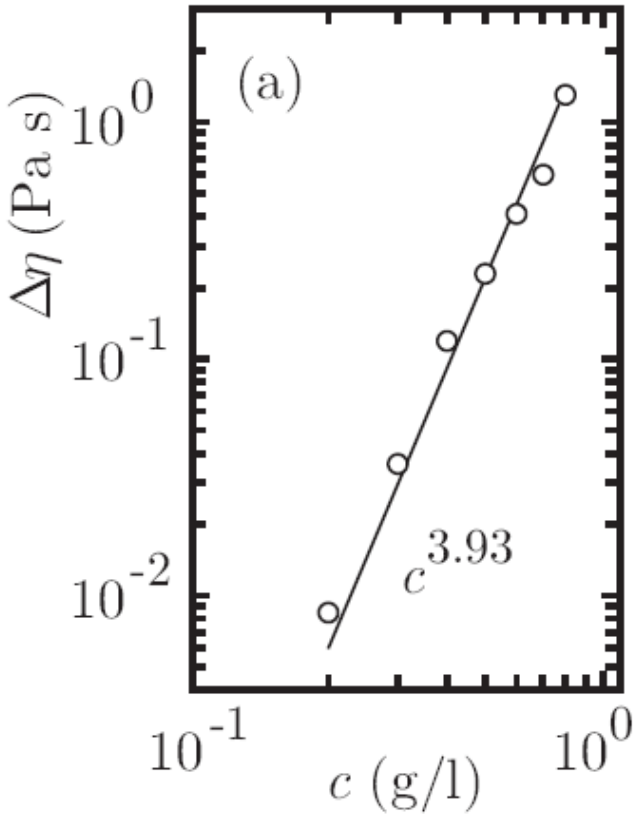

Fig. 3.3 Low shear viscosity increment $\Delta\eta$ versus DNA concentration c. The solid line represents the scaling law for a salted and entangled polyelectrolyte $\Delta\eta \simeq c^{3.93}$.

3.4.2 Viscoelastic moduli

The elastic storage and viscous loss moduli can be obtained from the mean square displacement according to Eq. [6]. For this purpose, it is also necessary to determine the derivatives α, β, and γ as defined in Eqs. [4]. Values of α, β, and γ were obtained by a 4th order polynomial fit to the data. The polynomial fits are also shown in Fig. 1 and they describe the smooth variation of the mean square displacements well. The resulting viscoelastic moduli are displayed in Fig. 2. The results for 0.7 and 0.5 g of DNA/L fall perfectly between the marks set by the 0.8, 0.6, and 0.4 g of DNA/L solutions and are not shown. We have checked that the second order approximation in β and γ calculated with coefficients c_1 through c_5 gives results which are slightly different than the ones obtained with a first order expansion with coefficients c_1 and c_2.

It should be noted that the viscoelastic moduli are derived based on the assumption that the DNA solution is homogeneous. In particular, depletion in DNA concentration in an interfacial region surrounding the bead with a thickness on the order of the mesh size is neglected. For concentrations in the range 0.03-0.4 g of DNA/l, Chen *et al*. have quantified the submicron scale variation in the viscoelastic response by using one and two-point tracking microrheology (11). It was shown that the viscoelstic moduli, as measured by

the single-particle method, are somewhat underestimated due to depletion. This effect becomes progressively less important with increasing DNA concentration (smaller mesh size) and/or larger bead diameter. We have checked that the viscoelastic moduli of a solution with a concentration of 0.35 g of DNA/l, as obtained from the tracking of 1.0 as well as 3.2 μ m sized beads, are very close. This can be understood on the basis of the small values of the correlation length less than 100 nm for concentrations exceeding 0.3 g of DNA/l (9). It is possible to correct for the effect of depletion by using the shell model of Levine and Lubensky (12). It is observed that the moduli obtained from the tracking of the 1.0 and 3.2 μ m sized beads collapse to single curves by assuming a layer of water surrounding the beads with a thickness of the correlation length (13). In principle, all viscoelasticity data in this thesis can be corrected according this procedure. It is found that the correction does not result in a change in qualitative behavior of the viscoelastic response, including the scaling behavior of the low shear viscosity, the number of entanglements per chain, and the relaxation time. Furthermore, the correction becomes vanishingly small due to the decrease in correlation length to a value around the persistence length for higher DNA concentrations in the entangled regime. Under the present experimental conditions, the effect of depletion is hence relatively unimportant and is not further pursued.

The low shear viscosity η can be derived from the behavior of the viscous loss modulus at low frequencies. If the mean square displacement is

given by $\left\langle \Delta x^2(t) \right\rangle = 2Dt$, an analytical calculation of the one sided Fourier transform gives for the viscoelastic moduli $G'' = \eta\omega$ and $G' = 0$. As can be seen Fig. 2, for low frequencies G'' approaches the linear scaling $\eta\,\omega$. The fitted values of the low shear viscosity η agree with those obtained above from the long time diffusive behavior of the mean square displacement.

With increasing frequency, the viscous loss modulus first increases, then levels off a bit, and eventually increases again. Qualitatively similar behavior has been observed in the shear stress versus shear rate of T4-DNA at comparable concentrations (7). Concurrently, the elastic storage modulus monotonously increases and eventually levels off to a constant high frequency plateau value. For a concentration exceeding 0.3 g of DNA/L, the elastic storage modulus becomes larger than the viscous loss modulus in an intermediate frequency range. This transition concentration is about ten times the overlap concentration from the dilute to the semi-dilute regime. From self-diffusion experiments of fluorescence labeled λ-phage DNA in TE buffer, the entanglement concentration was estimated to be around 0.6 g of DNA/L (5). As we will see shortly, the formation of entanglements for DNA concentrations exceeding, say 0.3 g/L can also be inferred from the high frequency limiting values of the elastic storage modulus (as well as from the concentration scaling of the low shear viscosity increment and the longest relaxation time). The development of plateau elasticity for large frequencies and a crossing of the viscous loss by the elastic storage modulus at a crossover

frequency ω_c for concentrations exceeding a critical entanglement concentration have been reported before for calf thymus DNA of polydisperse length (6, 9).

The viscous loss modulus shows dispersion at two different frequency scales. One process is characterized by a relaxation time on the order of a second, which becomes longer with increasing concentration. This process is the reptation dynamics of the DNA molecules in the entangled solution. Its correlation time can be considered as an entanglement disengagement time or tube renewal time. For T2 or T4-DNA at comparable concentrations the corresponding relaxation times are two orders of magnitude longer, in agreement with the higher molecular weight (164 or 166 vs. 48.5 kbp) (3, 7). The other process occurs at higher frequencies with a correlation time on the order of 0.1 s and is relatively insensitive to the DNA concentration. The high frequency dispersion is related to the Rouse dynamics of the entire DNA molecule inside the tube formed by the entanglements. Similar high frequency dispersion has been observed in the shear stress versus shear rate of T4-DNA (7). Unfortunately, the frame rate of our industrial video camera is not high enough to map out the Rouse dynamics at high frequencies. Accordingly, the viscoelastic behavior at high frequencies is not further persued. Here we focus on the formation of the entanglements and reptation dynamics in the lower frequency range.

3.4.3 Entanglements and reptation dynamics

With increasing frequency, the elastic storage modulus increases and approaches a limiting plateau value G. The number of entanglements per chain can be derived from the ratio of G and the elasticity modulus pertaining to the (hypothetical) non-entangled Rouse chain $G_R = \rho kT$ evaluated at the same molecular density ρ. The ratio G/G_R is proportional to the number of segments per chain divided by the average number of segments between entanglements, so that the number of entanglements per chain is given by $G/G_R - 1$ (1, 2, 14). G is obtained from the high frequency limiting values of the elastic storage moduli and the ratio G/G_R is set out in Fig. 3.4. The experimental values can be considered as under limits, because the elastic storage moduli might increase a bit for even higher frequencies outside the observation window. At low concentration, G/G_R is around unity in agreement with non-entangled dynamics. For concentrations exceeding 0.3 g of DNA/L, G/G_R increases and follows the scaling law for an entangled polyelectrolyte with screened electrostatics $G/G_R \simeq c^{1.31}$ ($\nu = 0.588$) (2, 3). The number of entanglements per chain at a concentration of 0.8 g of DNA/L is about 7. For a sample of 2 g of λ-phage DNA/L, approximately 22 entanglements per chain has been reported in the literature based on bulk rheology measurements (15). The latter value agrees with our

number of entanglements per chain, provided they are extrapolated to the relevant concentration according to $c^{1.31}$ scaling.

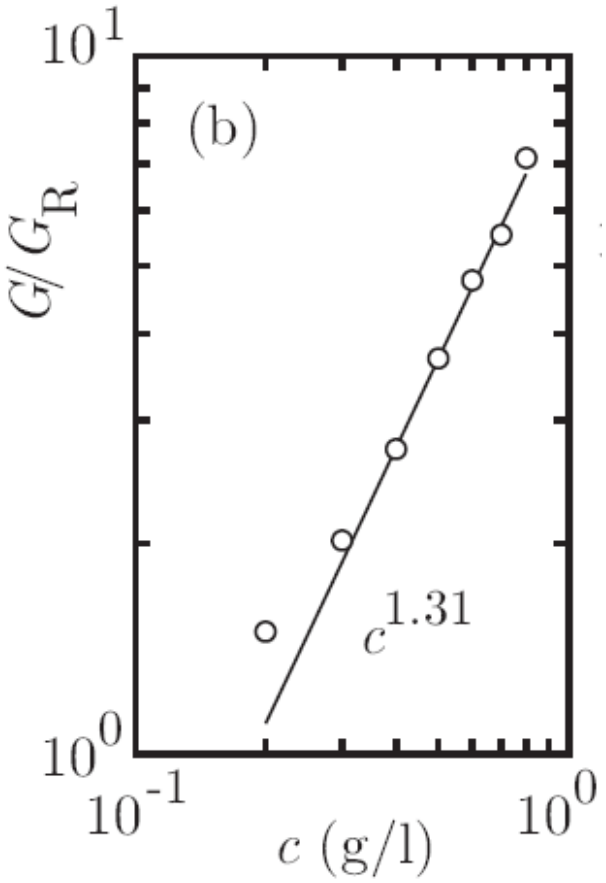

Fig. 3.4 High frequency elasticity modulus divided by the Rouse modulus G/G_R versus DNA concentration c. The solid line represents the scaling law of the number of segments per chain divided the average number of segments between entanglements $N/N_e \simeq c^{1.31}$.

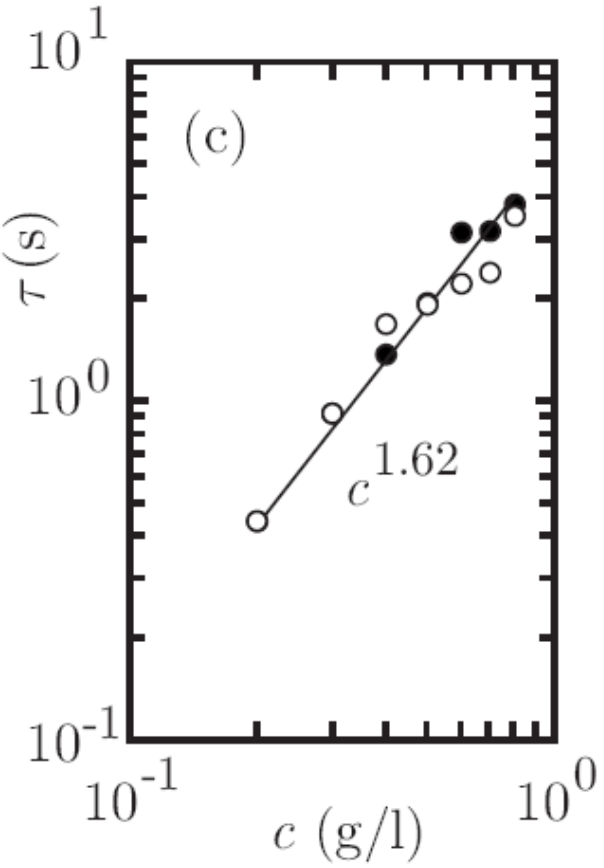

Fig. 3.5 Relaxation time τ versus DNA concentration c. The open circles refer to the values obtained from the low shear viscosities, whereas the closed circles represent the reciprocal lowest crossover frequencies. The solid line represents the scaling law $\tau \simeq c^{1.62}$.

The longest, global relaxation time can be obtained from the lowest crossover frequency of the viscous loss and elastic storage moduli $\omega_c = \tau^{-1}$ indicated by the arrows in Fig. 2. The results are displayed in Fig. 3.5. τ can be derived from either the increment in the low shear viscosity or the high frequency limiting value of the elastic storage modulus $\Delta\eta = \pi^2/12\, G\tau$ (14). The corresponding results are also displayed in Fig. 3.5. The values of the relaxation times obtained with both procedures agree within experimental accuracy. Note that the crossover frequency is only observed for entangled solutions (hence for concentrations exceeding 0.3 g of DNA/L), whereas the method based on the low shear viscosity is general and can also be used to derive the global relaxation of DNA molecules in the dilute and non-entangled semi-dilute regimes. The relaxation time increases by about an order of magnitude from 0.4 s for non-entangled DNA to about 4 s at the highest concentration in the entangled regime. Furthermore, the relaxation time follows the scaling law for reptation dynamics of a salted polyelectrolyte $\tau \simeq c^{1.62}$ ($\nu = 0.588$) (2, 3). For concentrations below the entanglement concentration, we do not observe the transition to Rouse dynamics with a much weaker concentration dependence $\tau_R \simeq c^{0.31}$. For this purpose, the measurements need to be extended to even lower values of the DNA concentration.

3.5 Conclusions

The viscoelastic moduli of λ-phage DNA through the entanglement transition was obtained with the help of particle tracking microrheology using minute samples of no more than 15 μL each. With increasing frequency, the viscous loss modulus first increases, then levels off, and eventually increases again. Concurrently, the elastic storage modulus monotonously increases and eventually levels off to a constant high frequency plateau value. Once the DNA molecules become entangled at about ten times the overlap concentration, the elastic storage modulus becomes larger than the viscous loss modulus in an intermediate frequency range. The number of entanglements per chain is obtained from the plateau value of the elasticity modulus. We cover the range from the non-entangled, semi-dilute to the moderately entangled regime with about seven entanglements per chain. The longest, global relaxation time pertaining to the motion of the DNA molecules is obtained from the low shear viscosity as well as from the lowest crossover frequency of the viscous loss and elastic storage moduli. In the entangled regime, both relaxation times agree and can be identified with the entanglement disengagement time or tube renewal time. The concentration dependencies of the low shear viscosity, the number of entanglements per chain, and the relaxation time agree with the relevant scaling laws for

reptation dynamics of entangled polyelectrolytes with screened electrostatics. The high frequency dispersion in the viscous loss modulus is relatively insensitive to the DNA concentration and is related to the Rouse dynamics of the DNA molecule inside the tube formed by the entanglements.

Reference

1. P. G. de Gennes. 1979. Scaling Concepts in Polymer Physics, Cornell University Press, Ithaca, NY.
2. J. R. C. van der Maarel. 2008. Introduction to Biopolymer Physics, World Scientific, Singapore.
3. Musti, R., Sikorav, J. R., D. Lairiez, G. Jannink, and M. Adam. 1995. Viscoelastic properties of entangled DNA solutions. C. R. Acad. Sci., Ser. IIb: Mec., Phys., Chim., Astron. 320: 599-605.
4. Heo, Y. and Larson, R. G. 2005. The scaling of zero-shear viscosities of semidilute polymer solutions with concentration. J. Rheol 49: 1117-1128.
5. Smith, D. E., Perkins, T. T. and Chu, S. 1995. Self-diffusion of an entangled DNA molecule by reptation. Phys. Rev. Lett 75: 4146-4149.
6. Mason, T. G., Dhopple, A. and Wirtz, D. 1998. Linear viscoelastic moduli of concentrated DNA solutions. Macromolecules 31: 3600-3603.
7. Jary, D., Sikorav, J. L. and Lairiez, D. 1999. Nonlinear viscoelasticity of entangled DNA molecules. Europhys. Lett 46: 251-255.

8. Mason, T. G. 2000. Estimating the viscoelastic moduli of complex fluids using the generalized Stokes-Einstein equation. Rheol. Acta 39: 371.

9. Verma, R., Crocker, J. C., Lubensky, T. C. and Yodh, A. G. 1998. Entropic colloidal interactions in concentrated DNA solutions. Phys. Rev. Lett 81: 4004-4007.

10. Mason, T. G., Ganesan, K., van Zanten, J. H., Wirtz, D. and S. C. Kuo. 1997. Particle tracking microrheology of complex fluids. Phys. Rev. Lett 79: 3282-3285.

11. Chen, D. T., E. R. Weeks, J. C. Crocker, M. F. Islam, R. Verma, J. Gruber, A. J. Levine, T. C. Lubensky, and A. G. Yodh. 2003. Rheological microscopy: Local mechanical properties from microrheology Phys. Rev. Lett. 90: 108301.

12. Levine, A. J. and Lubensky, T. C. 2001. Response function of a sphere in a viscoelastic two-fluid medium. Phys. Rev. E 63: 041501.

13. Bandyopadhyay, R. and A. K. Sood, Pramana. 2002. Rheology of semi-dilute solutions of calf-thymus DNA. J. Phys 58: 685.

14. Doi, M. and Edwards, S. F. 1986. The Theory of Polymer Dynamics. Oxford University Press, New York.

15. Teixeira, R. E., Dambal, A. K., Richter, D. H., Shaqfeh, E. S. G. and Chu, S. 2007. The individualistic dynamics of entangled DNA in solution. Macromolecules 40: 2461-2476.

Chapter 4

The effect of crowding on the conformation of supercoiled DNA from neutron scattering measurements and Monte-Carlo simulation

4.1 Introduction

DNA often exists in a supercoiled conformation, in which the duplex is wound around itself to form a higher order helix. Supercoiling is utilized in many cellular functions; examples include replication and transcription, formation of protein complexes, and alternate secondary structures such as cruciforms (1). It provides a mechanism for the site juxtaposition of distal segments of the same DNA molecule, which is important for gene expression. The conformation of the supercoil is determined by topological and geometrical properties, such as degree of interwinding and number of interwound branches. The topological constraint sets the spatial extent of the molecule and determines its excluded volume. Supercoiling has accordingly reported to be a major compaction mode for DNA in a crowded and congested state, such as in liquid crystals (2, 3), the nucleoid of a bacterial cell (4), or a

synthetic gene transfer vector (5). In order to be accommodated in the crowded state, supercoiled DNA has to decrease its excluded volume by a change in conformation. Correspondingly, the conformation is expected to depend on crowding through the effect of intermolecular interactions among DNA molecules at higher concentrations as well as through interactions with other bio-molecules including protein.

Supercoiled DNA can be visualized by (cryo-) electron and atomic force microscopy (6, 7, 8). It has been observed that the shape of the molecule is generally quite irregular, but that the average distance between the opposing duplexes in the supercoil (interduplex distance D_{sc}) is inversely proportional to the superhelical density and decreases with increasing ionic strength of the supporting medium. These imaging techniques are however not well adapted to the investigation of typical three-dimensional solution properties, such as excluded volume, which control the packing of DNA in a crowded state. Typical size-related properties are best and quantitatively inferred from scattering experiments of DNA dispersed in a relevant buffer. The interwound conformation of a small plasmid (pUC18, 2686 bp) has previously been investigated with small angle neutron scattering (SANS) (9, 10). It was found that D_{sc} decreases with increased salt and/or DNA concentration. These experiments may however be compromised by the contribution to the

scattering from inter-DNA interference; in particular, those experiments involving samples with higher plasmid and lower salt concentrations. Inter-DNA interference may obscure the information on the conformation. In the study here, inter-DNA interference was eliminated by performing SANS experiments in the condition of zero average DNA neutron scattering contrast.

4.2 Neutron scattering contrast variation

In SANS studies, contrast variation is often used to blank out or highlight certain molecular components of a large system. The scattering contrast is therefore a key experimental parameter. In the case of DNA, the scattering length contrast of the nucleotides with respect to solvent (water) is given by

$$\overline{b}_{DNA} = b_{DNA} - b_s \, \overline{v}_{DNA} / \overline{v}_s \quad . \qquad [1]$$

Here, b_{DNA} and b_s are the scattering lengths of a nucleotide and solvent, respectively. Note that the relevant parameter is the contrast per unit volume, so that the subtracted scattering length of the solvent has to be multiplied with the ratio of the corresponding partial molar volumes $\overline{v}_{DNA} / \overline{v}_s$. In a mixture of H_2O and D_2O, the scattering length of the solvent is

$$b_s = X b_{D_2O} + (1 - X) b_{H_2O} , \qquad [2]$$

where X is the mole fraction of D_2O. Our SANS experiments were performed under full (100% H_2O) and zero (9% H_2O, 91% D_2O) average

DNA contrast conditions. Fully hydrogenated plasmid (DNA^H) was used for the full contrast experiment. In the case of the zero average contrast experiment, a 50% mixture of DNA^H and the perdeuterated plasmid (DNA^D) was used. The values of the scattering lengths of the hydrogenated and perdeuterated nucleotides b_{DNA^H} and b_{DNA^D}, respectively, are different (see Table I) due to the difference in scattering lengths of hydrogen and deuterium (11). We will use this phenomenon, together with contrast variation in the solvent, to realize the zero average contrast condition. In this condition, $\bar{b}_{DNA^H}$ and $\bar{b}_{DNA^D}$ have the same absolute value, but with opposite sign.

For our samples, the small angle scattering is dominated by DNA. The contribution from the small ions is negligible (12). In the condition of full contrast, the scattering intensity is given by

$$I_{FC}(q) = \rho\, \bar{b}_{DNA}^2\, S(q). \qquad [3]$$

with ρ the nucleotide density. We used hydrogenated plasmid DNA^H in 100% H_2O, so that $\bar{b}_{DNA} = \bar{b}_{DNA^H}$. The momentum transfer q is defined by the wavelength λ of the radiation and the angle θ between the incident and scattered beam according to $q = (4\pi/\lambda)\sin(\theta/2)$. The static structure factor $S(q)$ is the spatial Fourier transform of the DNA density correlation function and can be expressed as a sum of an intra- $P(q)$ and an intermolecular $H(q)$ part:

$$S(q) = P(q) + \rho H(q). \quad [4]$$

As q is increased, the intermolecular part $H(q)$ becomes progressively less important and the structure factor $S(q)$ asymptotically approaches the statistically averaged, single-molecule form factor $P(q)$. It should be noted that $P(q)$ depends on the environmental conditions of the dispersed plasmid through the effects on the three-dimensional structure. In SANS experiments, the intermolecular contribution $H(q)$ cannot usually be neglected and complicates the interpretation of the full contrast scattering intensities in terms of molecular structure (12). By analogy with the convention for systems with spherical symmetry, we define the solution structure factor by taking the ratio of the total structure and the form factor

$$S(q)/P(q) = 1 + \rho\, H(q)/P(q). \quad [5]$$

Note that the solution structure factor approaches unity for large values of momentum transfer and/or low densities due to vanishingly small intermolecular interference.

The effect of intermolecular interference can be eliminated by carrying out an experiment in the zero average contrast condition (13, 14). For maximum intensity, we have employed a 1:1 mixture (by mole) of DNA^{H} and perdeuterated plasmid DNA^{D}. It is assumed that the structure does not depend

on the isotopic composition of the plasmids. For such a mixture, the scattering intensity is given by (15)

$$I(q) = \rho\left[(\bar{b}^2_{DNA^H} + \bar{b}^2_{DNA^D})P(q)/2 + \rho(\bar{b}_{DNA^H} + \bar{b}_{DNA^D})^2 H(q)/4\right]. \quad [6]$$

In the condition of zero average contrast, *i.e.* $\bar{b}_{DNA^D} = -\bar{b}_{DNA^H} = \bar{b}_{DNA}$, the intermolecular contribution $H(q)$ is seen to vanish. From Eqs. [1] and [2] and the data in Table 1, it follows that this condition is realized in a solvent mixture of 9% H_2O and 91% D_2O (by volume). The intensity is then directly proportional to the single molecule form factor

$$I_{ZAC}(q) = \rho\, \bar{b}^2_{DNA}\, P(q). \quad [7]$$

irrespective the concentration of DNA.

Table 4.1: Partial molar volumes $\bar{v}$ and neutron scattering lengths *b*.

	$\bar{v}$ (cm^3/mole)	b (10^{-12} cm)
DNA^H	172	9.81+2.02 x [a]
DNA^D	172	19.52+2.02 x
H_2O	18	−0.168
D_2O	18	1.915

[a] x denotes the D_2O mole or volume fraction (effect of exchangeable hydrogen).

The form factor averaged over all orientations is defined as

$$P_{sc}(q) = \frac{1}{N}\sum_{i=1}^{N}\sum_{j=1}^{N}\left\langle \frac{\sin qr_{ij}}{qr_{ij}} \right\rangle. \qquad [8]$$

where r_{ij} is the distance between two nucleotides of a single DNA molecule. An average needs to be taken over all conformations. The form factor is normalized at $q = 0$ to the number N of nucleotides per DNA molecule (for pHSG298 $N = 5350$). At different values of momentum transfer, the form factor provides information about the conformation of the supercoil at correspondingly different length scales. The plectonemic interwinding is characterized by radius r (interduplex distance $2r$) and pitch $2\pi p$. It should be noted that the shape of the supercoil is generally quite irregular and that there is significant fluctuation in radius and pitch. In the very low q range, the scattering is sensitive to long range structural effects such as branching and overall flexibility of the superhelical axis.

For very high values of q, the scattering is essentially given by a single duplex of the superhelix. The high q limiting form of the form factor is given by

$$P_{sc}(q) = N\pi P_c / ql \quad , \quad (qr \gg 1,\ qp \gg 1). \qquad [9]$$

with l the contour length of the DNA molecule and

$$P_c(q) = \left[2J_1(qr_p)/(qr_p)\right]^2. \qquad [10]$$

expresses the effect of the cross-sectional radius of gyration r_p of the duplex.

In the intermediate q range with $qr \approx 1$ and $qp \approx 1$, the form factor shows a characteristic oscillation with a broad minimum and subsequent maximum if it is normalized in such a way that it goes to unity at high q. This feature is due to intra-superhelix interference both in the radial and longitudinal direction over lengths r and p, respectively.

4.3 Materials and methods

4.3.1 Preparation of perdeuterated cell paste

The cell paste for the isolation of perdeuterated plasmid DNA was prepared at the ILL-EMBL Deuteration Laboratory, Grenoble, which is optimized for the production of both selectively and non-selectively deuterated biomolecules (16, 17). BL21 (DE3) cells were transformed with pHSG298. Adaptation of BL21 (DE3) pHSG298 cells to deuterated medium was achieved by an adaptation process on minimal medium agar plates. Cells were grown in deuterated minimal medium containing 40 mg/L kanamycin (18, 19, 20). For preparation of fully deuterated medium, mineral salts were dried in a rotary evaporator (Heidolph) at 60 ^{o}C and labile protons exchanged for deuterons by dissolving them in a minimal volume of D_2O and subsequent redrying. Perdeuterated d_8-glycerol (Euriso-top, France) was used as a carbon source. A preculture of 150 cm^3 adapted cells were used to inoculate 1.3 L

deuterated minimal medium in a 3 L fermenter (Labfors, Infors). During the batch and fed-batch phases, the pH was adjusted to 6.9 by addition of NaOD (Euriso-top, France) and the temperature to 30 ^{o}C. The gas-flow rate of sterile filtered air was 0.5 L per minute. Stirring was adjusted to ensure a dissolved oxygen tension of 30%. The fed-batch phase was initiated when the optical density at 600 nm reached a value of 4. D_8-glycerol was added to the culture to keep the growth rate stable during fermentation. When OD_{600} reached a value of 15, cells were harvested and stored at -80 ^{o}C From 2 fermenter runs, 92 g of deuterated cell paste was obtained. 45 g of the paste was used for the extraction of perdeuterated plasmid.

4.3.2 Preparation of hydrogenated cell paste

For the hydrogenated cell paste, BL21 bacteria transformed with pHSG298 were grown on a Luria Broth plate with kanamycin (25 mg/L). A single colony was taken to grow a starter culture in Luria Broth medium containing kanamycin at 37 ℃ for eight hours (OD_{600} = 0.8). The starter culture was then diluted 1000 times into Luria Broth medium containing kanamycin and grown at 37 ℃ for 12–16 h with vigorous shaking (300 rpm, OD_{600} = 1.8 for each batch). The bacterial cells were harvested by centrifugation at 6000 *g* for 15 min at 4 ℃. The cell pellet was weighed and 60 g was taken for the extraction of plasmid in the hydrogenated form.

4.3.3 Plasmid extraction

The bacterial pellets were suspended in 0.5 L of 50 mM Tris-HCl buffer, pH 7.5, 10 mM EDTA and subsequently lysed with 0.5 L of an alkaline solution (0.2 M NaOH, 1% SDS) at room temperature. The pH of the cell suspension and the alkaline solution was maintained below 12.5. Bacterial genomic DNA, cell debris, and proteins were precipitated by the addition of 0.5 L of 3 M potassium acetate, pH 5.5, pre-chilled at 4 ℃. After centrifugation at 20,000 *g* for 30 minutes at 4 ℃, the supernatant was pumped through a Sepharose 6 fast flow column (XK 50/30) equilibrated with 2 M $(NH_4)_2SO_4$, 10 mM EDTA, and 100 mM Tris–HCl, pH 7.0 with an AKTA explorer chromatography system (GE Life Sciences, columns and chromatography media were also purchased from GE). This gel filtration step results in the removal of RNA. The plasmid was further purified by thiophilic interaction chromatography using a column packed with PlasmidSelect equilibrated with the above mentioned 2 M $(NH_4)_2SO_4$ buffer and eluted with a gradient to 0.4 M NaCl, 2 M $(NH_4)_2SO_4$, 10 mM EDTA, and 100 mM Tris–HCl, pH 7.0 (21). Finally, the sample was concentrated and endotoxins were removed by capturing the plasmid on a Source 30Q ion exchange column followed by elution in a gradient to 0.6 M NaCl. After precipitation with

isopropanol, the DNA pellet was gently dried for a short period and dissolved in TE buffer (10mM Tris, 1mM EDTA, pH 8) and stored at 4 ℃.

4.3.4 Plasmid characterization

UV spectroscopy showed that the ratio of the optical absorbance at 260 nm and 280 nm (A260/A280) exceeded 1.8, indicating that the preparations were free of protein. The integrity of the plasmids was checked with 1% agarose gel electrophoresis in TAE buffer (40 mM Tris-acetate, 1 mM EDTA, pH 8.3) at 70 V for 2 hours (22). The linking number deficit and percentage of open circular plasmids were determined by 1.4% agarose gel electrophoresis in TPE buffer (90 mM Tris-phosphate, 1 mM EDTA, pH 8.3) with duplex unwinding chloroquine at 50 V for 36 hours (23). The chloroquine concentration was increased from 1 to 120 mg/L. An optimal separation of the topoisomers was observed at chloroquine concentrations of 3 mg/L and 80 mg/L. At these concentrations all molecules are either negatively or positively supercoiled. The position of the band pertaining to $\Delta Lk = 0$ was determined by relaxation of the plasmid with topoisomerase type II. The most probable $\Delta Lk = -9 \pm 2$, which is close to the average value pertaining to the whole population. We have checked that the superhelical densities of the hydrogenated and perdeuterated plasmids are similar, but the distribution in

hydrogenated topoisomers extends over a slightly broader range of ΔLk, as shown in Chapter 2.

4.3.5 Sample preparation

All sample manipulations involving D_2O were performed under a flow of Argon in order to minimize exchange with atmospheric water. All DNA concentrations are determined by weight and checked with UV spectrometry. Standard quartz cuvettes with 0.1 or 0.2 cm path length were used for full and zero average contrast experiments, respectively. The DNA scattering length depends on the base composition, because different bases have different atomic compositions (11). The mean values was calculated according to the pHSG298 base composition (NCBI database, accession number M19415). The results are noted in Table 1, together with the scattering lengths of the solvents and partial molar volumes. For hydrogenated plasmid in H_2O, the full contrast $\overline{b}_{DNA} = 11.4 \times 10^{-12} cm^{-1}$. The zero average DNA contrast $\overline{b}_{DNA} = 4.85 \times 10^{-12} cm^{-1}$ is realized for a 1:1 mixture by mole of hydrogenated and deuterated plasmid in 9% H_2O and 91% D_2O by volume.

4.3.6 Small angle neutron scattering

SANA experiments were performed using the D11 diffractometer, on the cold source of the high neutron flux reactor at the the Institute Laue Langevin,

Grenoble. The sample temperature was 298 K. A wavelength of 0.6 nm with a 10% spread was was selected, and the distances between the sample and the planar square multidetector (sample-detector, (*S*-*D*) distance) were 1.1, 4.0, and 13.5 m, respectively. This allows a momentum transfer range of 0.04 to 3 nm^{-1}. The total counting times for all detector settings was approximately 2 hours per sample. Data reduction allowed subtraction of background scattering, sample transmission, and detector pixel efficiency. The efficiencies of the detector pixels were determined using the scattering of H_2O. Absolute intensities were obtained by reference to the attenuated direct beam.

4.3.7 Computer simulation

The Monte-Carlo simulation was done by my colleague, Ng Siow Yee. The computer code for the model Hamiltonian, including the interaction with the confining cylindrical volume was programmed using FORTRAN 90 and it was executed on a cluster of 3 GHz Xeon 2 dual core processors. For each ionic strength, it started with the simulation of the free supercoil with $\lambda = 0$. The initial conformation was a regular ring with zero writhing number. Subsequently, a series of simulations was done with progressively smaller values of D_{cyl} ranging from 40 to 10 nm with an increment of 5 nm. In a second round of simulations, we have used optimized values of D_{cyl}, i.e. 5.6, 6.4, 7.7, 11.2 nm for 4 mM, 3.6, 4.3, 5.1, 9.8 nm for 20 mM, and 5.3, 6.5, 6.1,

7.2 nm for 100 mM ionic strength. For each cylinder diameter, the parameter λ was incremented from 1×10^{-5} to 1 in 10 logarithmically spaced steps. In the presence of the confining potential, the initial conformation was always taken to be the equilibrated conformation pertaining to the previous run. Small random displacements were applied on each vertex with an acceptance ratio of 50%. The simulation was considered to have reached equilibrium when the radii of gyration R_g of the DNA molecule pertaining to two consecutive runs with a total of 16×10^6 cycles agreed within 95% confidence level. Once the system reached equilibrium another 24×10^6 cycles were performed. Hence 40×10^6 Monte Carlo cycles were executed, which correspond with 40×10^3 conformations for each condition specified by cylinder diameter and ionic strength. With this ensemble of conformations, we calculated the form factor and the distance distribution function of the vertices. The writhing number *Wr* was obtained by the evaluation of the Gauss double integral. A typical run for one cylinder diameter and ionic strength took about 1 month.

4.4 Results and discussion

4.4.1 Neutron scattering measurements

The structure factors *S(q)* and form factors *P(q*) pertaining to the lowest and highest DNA concentrations with various concentrations of salt are

displayed in Fig.1. For samples with higher DNA and/or lower salt concentration, increasingly important intermolecular interference results in an increased suppression of *S(q)* at smaller *q* values. This suppression is not seen in *P(q)*. In the limit $q \rightarrow 0$, *P(q)* agrees with the number of nucleotides per plasmid N=5350. This low q limiting behavior confirms the elimination of intermolecular interference in the zero average contrast condition. As q is increased, the difference between *S(q)* and *P(q)* becomes vanishingly small, because intermolecular interference becomes progressively less important at smaller distance scales. All samples show significant intermolecular interference, even down to 6 g of DNA/L in 100 mM of NaCl. These results show that intermolecular interference can only be neglected for even less concentrated solutions with excess salt. It should be noted that at high DNA concentration, the effect of salt on *S(q)* is minimal. This indicates that the intermolecular interaction is mainly determined by the spatial extent of the plasmid (excluded volume), rather than screened electrostatics. Because there are not good models available describing intermolecular interaction of supercoiled DNA, further interpretation of *S(q)* is refrained. Here, we focus on *P(q)* and, in particular, how we can obtain the interduplex distance D_{sc} as a function of salt and DNA concentration.

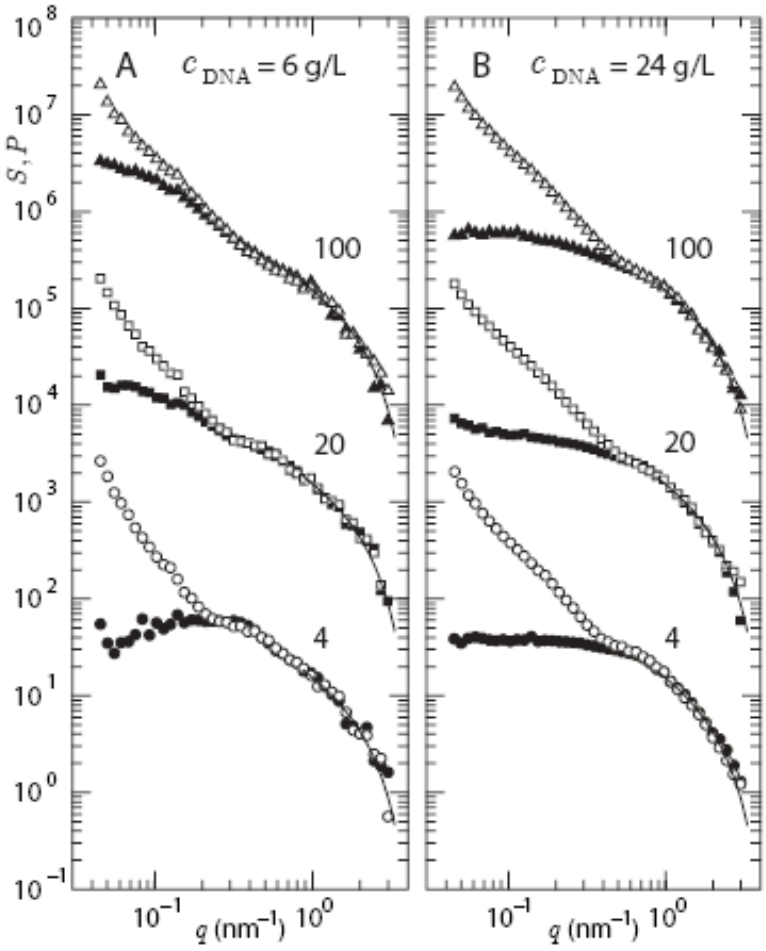

Fig. 4.1 Form factor P (open symbols) and structure factor S (closed symbols) versus momentum transfer *q*. The DNA concentrations are 6 (A) and 24 g/L (B). The NaCl concentrations are indicated in mM. The solid curves represent the form factor P_d pertaining to the duplex with a cross-sectional radius of gyration rc = 0.8 nm. To avoid overlap, the data are shifted along the y-axis with a multiplicative constant.

In the double logarithmic representation and with increasing values of *q*, *P(q)* first decrease, then tends to level off. After that, it decreases again. For high *q* values, *P(q)* is seen to converge to the expression pertaining to a locally rodlike duplex $P_d(q) = N\pi P_c/(ql)$ with l the contour length of the DNA molecule and $P_c(q) = [2J_1(qr_c)/(qr_c)]^2$ represents the effect of the cross-sectional radius of gyration r_c (14, 24). The effect of salt and DNA concentration on the conformation of the plasmid is more clearly illustrated if *P(q)* is normalized in such a way that it goes to unity at high *q*, i.e., for *P(q)* divided by $P_d(q)$. The results are displayed in Fig. 4.2. The normalized form factor P/P_d show an oscillation with a broad minimum and subsequent maximum. This oscillation is due to intramolecular interference in both the radial and longitudinal direction over the diameter and pitch of the superhelix, respectively (10). In particular, the positions of the extrema along the q-axis are inversely proportional to the distance D_{sc} between the two opposing duplexes of the supercoil. With increasing DNA and/or salt concentration, the positions of the extrema shift to higher *q* values. This shift shows qualitatively that the plasmid becomes more compact in the lateral direction with a smaller value of D_{sc}. The signature oscilation is largely obscured in the normalized structure factor S/P_d due to intermolecular interference.

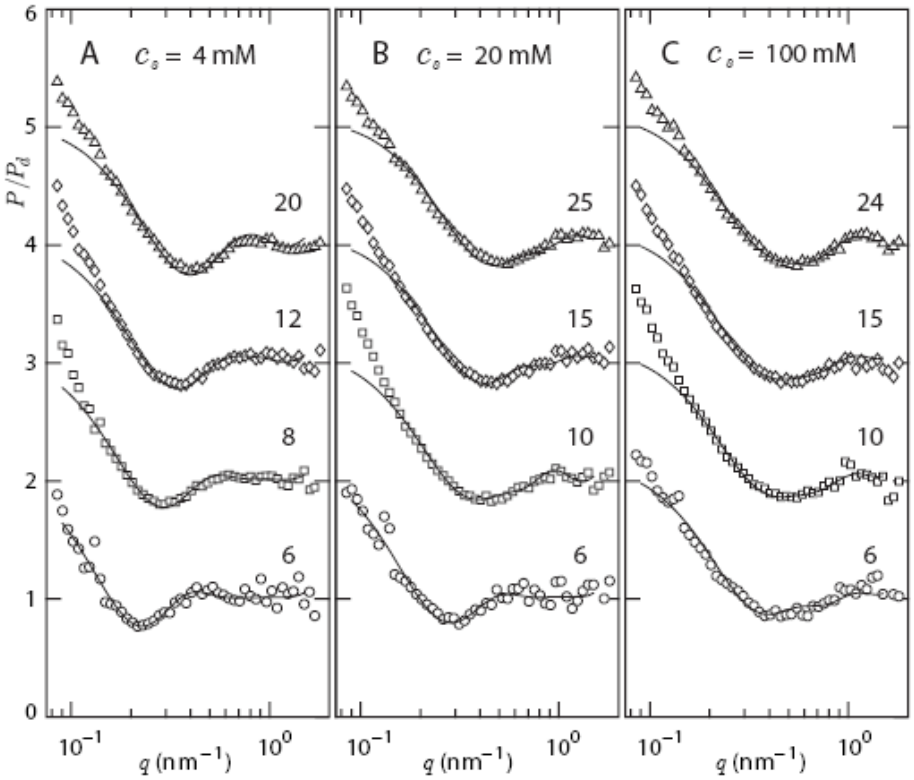

Fig. 4.2 Normalized form factor P/P_d versus momentum transfer q. The NaCl concentrations c_s = 4 (A) and 20 (B), and 100 mM (C). The DNA concentrations are indicated in g/L. The curves are the simulated normalized form factors $\bar{P}_{sc}/P_v$ with interduplex distances D_{sc} as shown in Fig. 5. To avoid overlap, the data are shifted along the y-axis with an incremental constant.

4.4.2 Monte-Carlo simulation

Quantitative information about the interduplex distance D_{sc} is derived by comparing the SANS form factors with the results of Monte-Carlo computer simulation (simulations were done by my colleague Ng Siow Yee). In the simulation, the DNA molecule was modeled as a closed circular, polygonal space curve consisting of 293 elastic vertices with mean bond length $\langle b \rangle = 3.1$ nm, contour length $l = 910$ nm, and linking number deficit $\Delta Lk = -9$ (25, 26). It has been checked that a variation in ΔLk from -9 to -4 has a negligible effect on the derived values of D_{sc}. The twisting and bending flexibility of the space curve is characterized by persistence length L_t and L_b, respectively. The usual value for the bending persistence length $L_b = 50$ nm. The elasticity constant for twisting of the duplex is not precisely known. For weakly strained, circular DNA, the experimental values of L_t, as obtained from fluorescence depolarization anisotropy measurements, are around 50 nm (27). Accordingly, simulations were performed with $L_t = 50\ nm$ ($L_b = L_t$).

The vertices interact through the sum of a hard sphere (diameter $\sigma_D = 2.4$ nm) and an isotropic, screened Coulomb potential

$$V(r) = (\frac{\sigma_D}{r})^{12} + l_B \alpha^2 \frac{exp(-\gamma_D r)}{r}. \quad [12]$$

Note that this potential includes the short-range electrostatic repulsion and there is no need to modify the bending persistence length. The strength and

range of the electrostatic interaction are determined by the Bjerrum length l_B, effective number of charges per vertex $\alpha = \nu_{eff}\langle b\rangle$, and screening length λ_D^{-1}, respectively. $\alpha = 6.7, 10,$ and 22 were obtained by numerically solving the non-linear Poisson Boltzmann equation for a rod-like polyelectrolyte of 2.4 nm diameter in 4, 20, 100 mM of a monovalent salt with λ_D^{-1} = 4.8, 2.2, and 1.0 nm, respectively (28).

The inclusion of the effect of crowding in the simulation protocol of supercoiled DNA is non-trivial and has not been done before. A test molecule is assumed to be effectively confined in a cylindrical volume by the surrounding molecules. This situation is the same as confinement in a straight nanochannel (25). Accordingly acylindrical potential $V_{cyl} = k_{cyl}\sigma_D r_{cyl}^{10}$ is applied, with radial coordinate r_{cyl}. This potential is a good approximation for hard-wall repulsion without causing computational difficulties. The value of k_{cyl} is determined by the diameter of the volume of confinement D_{cyl} and was chosen so that the energy of a contact per vertex with the confining wall equals k_BT. a description of intermolecular interaction in terms of a cylindrical volume of confinement is a simplification and ignores, e.g., fluctuation in DNA densit and possible interpenetration of the molecules. To account for these effects in an approximate way, the simulated form factors will be averaged over a distribution in D_{cyl}. The model also ignores long range

structural effects such as overall flexibility and branching of the superhelical axis. Nevertheless, we expect that a cylindrical potential of confinement captures the main effect of the reduction in available free volume resulting from crowding at a distance scale on the order of D_{sc}.

Simulations were performed with D_{cyl} in the range 7 to 40 nm. The most probable interduplex distance D_{sc} was obtained from the position of the maximum in the distance distribution function $p_v(r_{ij})$, where r_{ij} is the distance between two vertices. An example of p_v, as well as a snapshot of the equilibrated conformation, is displayed in Fig. 3. From the ensemble of conformations, the simulated form factor $P_{sc}(q)$ was calculated with Equation. 8. This procedure hence provides $P_{sc}(q)$ with the corresponding D_{sc} for each condition specified by cylinder diameter and ionic strength. The simulated form factors were subsequently averaged over a Gaussian distribution in D_{cyl} and convoluted with the resolution function of the diffractometer. The mean value and variance of D_{cyl} were optimized with the help of spline interpolation, so that the simulated averaged form factor $\bar{P}_{sc}$ is in fair agreement with the experimental result.

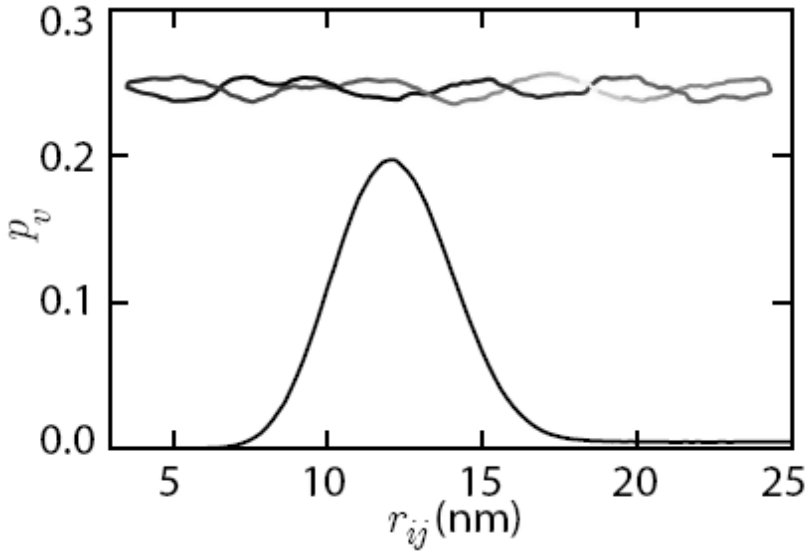

Fig. 4.3 Distribution function p_v versus the intervertex distance r_{ij} for $D_{cyl} = 20$ nm and c_s = 20 nm. The most probable distance $D_{sc} = 12$ nm. Correlations over distance scale less than the bending persistence length (20 vertices) are excluded. The inset is a snapshot of an equilibrated conformation after 16×10^6 cycles.

4.4.3 Analysis of the form factor

For high q values, $\bar{P}_{sc}(q)$ converges to the form factor of the vertex $P_v(q)$. All simulated $\bar{P}_{sc}/P_v$ are shown in Fig. 4.2. The optimized values of D_{cyl}, including its variance, are displayed in Fig. 4.4. The corresponding D_{sc} is shown in Fig. 4.5. In the relevant range of $q > 0.1\,\mathrm{nm}^{-1}$, overall good agreement between the experimental and simulated normalized form factors is observed. In particular, the positions of the broad minimum and subsequent maximum along the q-axis are well predicted. The distribution in D_{cyl} reduces the amplitude of the oscillation in $\bar{P}_{sc}/P_v$, but its width has no significant effect on the positions of the extrema nor the mean values of D_{sc}. The deviations in the low q range are due to long range structural effects such as overall flexibility and branching of the superhelical axis, which are not described by the model of confinement in a straight cylindrical volume.

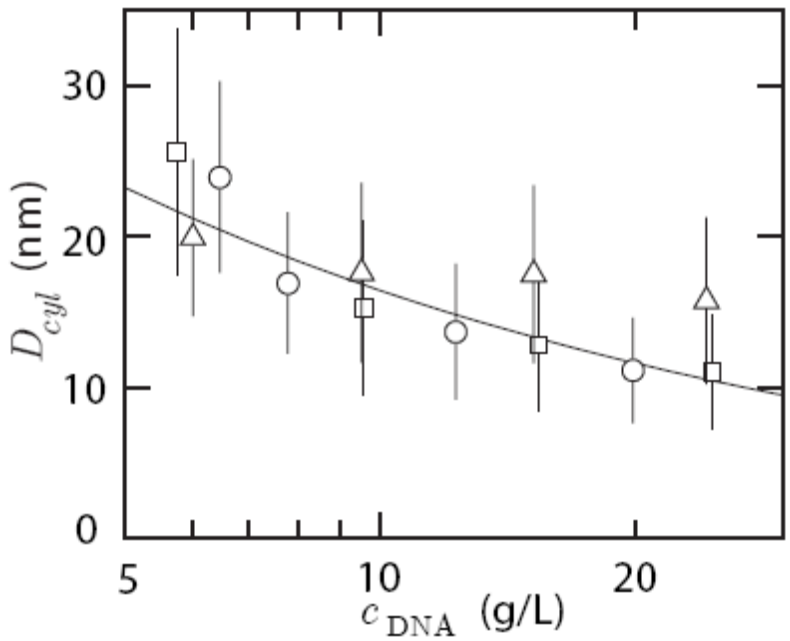

Fig. 4.4 Cylinder diameter D_{cyl} versus DNA concentration $c_{DNA.}$ The bars indicate the variance. The NaCl concentrations are 4 (○), 20 (□), and 100 (△) mM. The solid curve is the lateral intermolecular distance D_{lat} for closely packed wormlike cylinders.

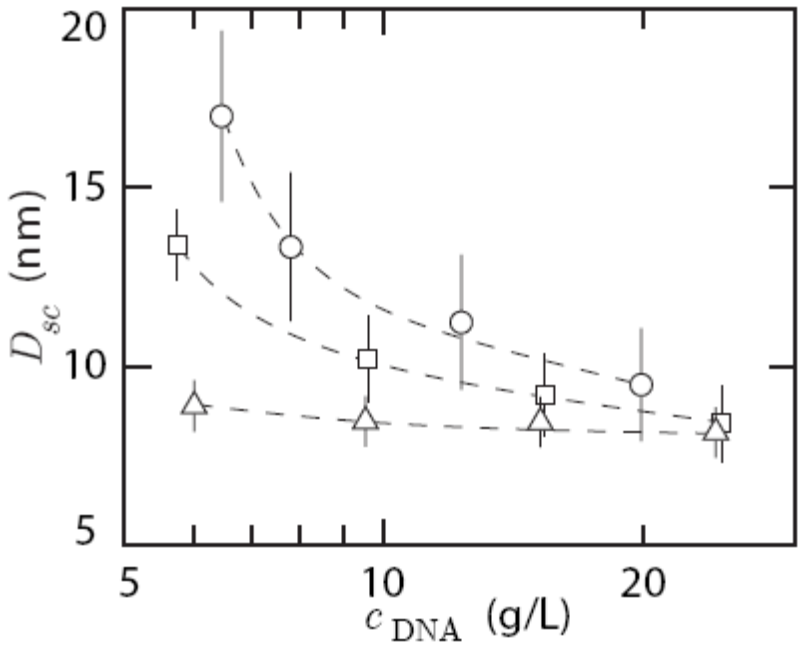

Fig. 4.5 As in Fig. 4.4, but for the interduplex distance D_{sc}. The dashed curves are guides to the eyes.

As shown in Fig. 4.4, the optimized values of D_{cyl} decrease with increasing DNA concentration and are in agreement with the average lateral intermolecular distance D_{lat} if the congested plasmids are seen as closely packed wormlike cylinders. With nucleotide density ρ and a spine-axis projected distance between the nucleotides $\mathrm{h} = 0.171\ \mathrm{nm}$, D_{lat} follows from $\rho^{-1} = 0.8\, hD_{lat}^2\pi/8$. The factor 0.8 accounts for the typical contraction of the superhelical axis caused by the plectonemic interwinding of the duplex (6). The variance in D_{cyl} is around 30%, due to the soft confinement imposed by surrounding molecules. The corresponding optimized values of D_{sc} decrease with increasing plasmid and salt concentration. A decrease in D_{sc} of a diluted supercoil with increasing ionic strength has previously been observed with electron (6, 7) and atomic force microscopy (8), sedimentation and catenation experiments (29, 30), SANS (9, 10), as well as computer simulations (31, 32, 33, 34). The magnitude and ionic strength dependence of D_{sc} agree with these previously reported results, as well as theoretical predictions based on the wormlike chain model (28, 35). It was also observed that D_{sc} decreases with increasing plasmid concentration. For the first time, these observations were made under crowded conditions without complication from intermolecular interference (zero average contrast). The decrease in D_{sc} with increased crowding depends on ionic strength and is most prominent in

conditions of minimal screening. Screened electrostatics is hence of paramount importance in determining the excluded volume, despite its relative unimportance for electrostatic intermolecular interaction. At high DNA concentration the limiting value of D_{sc} is around 8 nm, in accordance with the closest distance of two opposing segments of the interwound duplex with their respective double layers.

4.5 Conclusions

With a view to determining the distance between the two opposing duplexes of supercoiled DNA, the small angle neutron scattering from pHSG298 plasmid (2675 bp) in saline solutions were measured as a function of plasmid and salt concentration. Experiments were carried out using solvent contrast variation in conjunction with full and zero average DNA contrast. In the case of full contrast, the scattering intensity is proportional to the structure factor, which includes contributions from intra- and intermolecular interference. For the first time, the use of zero average DNA contrast has allowed the plasmid form factor to be obtained in a crowded solution without the contribution from intermolecular interference. A comparison of structure and form factors shows that intermolecular interference cannot be neglected in the present ranges of DNA concentrations and ionic strength. At high DNA

concentration the effect of salt on the structure factor is minimal. This shows that the intermolecular interaction is mainly determined by excluded volume, rather than screened electrostatics. It should be noted that this does not imply that screened electrostatics is not important, because it determines to a large extent the excluded volume though the intramolecular effect on the size of the plasmids. Due to the lack of good models describing intermolecular organization of supercoiled DNA, we have refrained from further interpretation of the structure factor in terms of, e.g., the random phase approximation and virial coefficients (24).

For high values of momentum transfer, the form factor converges to the form factor of the duplex. Clear intra-molecular interference is observed, once the form factor is normalized to the one of the duplex. The normalized form factors show a signature oscillation with a broad minimum and subsequent maximum. The positions of the extrema shift to higher values of momentum transfer with increasing DNA and/or salt concentration, which indicates compaction of the plasmid in the lateral direction with a concurrent decrease in interduplex distance. Quantitative information about the interduplex distance was derived by a comparison of the SANS form factors with the ones resulting from Monte-Carlo simulation. In the simulation, the many body problem of a dense solution was reduced to the one of a single molecule

confined in a cylindrical volume. The diameter of the volume of confinement is essentially determined by the average lateral intermolecular distance and its variance accounts for softness in confinement. As in previous reports (6, 7, 8, 9, 29, 31, 32, 33, 34), it's observed that the interduplex distance decreases with increasing salt concentration. It was also observed that the interduplex distance decreases with increasing DNA concentration. The crowding effect is highly sensitive to the salt concentration and is most significant in the condition of minimal screening. Accordingly, besides screened electrostatics, crowding is of importance in controlling the conformation of supercoiled DNA. For high salt and/or DNA concentration, the interduplex distance takes a value of around 8 nm. The site juxtaposition of distal DNA segments of supercoiled DNA in a crowded state such as in the cytoplasm of bacteria might have implications for gene regulation.

This study required the investigation of concentrated solutions, which in full contrast scattering experiments are prone to artifacts due to effects of intermolecular interference. The contribution of inter-DNA interference was eliminated by exploiting zero average DNA neutron scattering length contrast. This was made possible through the use of perdeuterated plasmid. This chapter has shown that the tertiary structure of DNA can be investigated closer to the native state in physiologically relevant conditions. This aspect is particularly

promising from biophysical and biotechnological points of view, e.g., for the investigation of the effect of DNA-protein interaction on the conformation of DNA.

References

1. Bloomfield, V. A., D. M. Crothers, and I. Tinoco. 2000. Nucleic acids; structure, properties and functions. University Science Books, Sausilito.

2. Reich, Z., E. J. Wachtel, and A. Minsky. 1994. Liquid-crystalline mesophases of plasmid DNA in bacteria. Science 264: 1460-1463.

3. Zakharova, S. S., Jesse, W., Backendorf, C., van der Maarel J. R. C. 2002. Liquid crystal formation in supercoiled DNA solutions. Biophys J 83: 1119-1129.

4. Cunha, S., Woldringh, C. L., Odijk, T. 2001. Polymer-mediated compaction and internal dynamics of isolated Escherichia coli nucleoids. J. Struct. Biol 136: 53-66.

5. Korobko, A. V., Backendorf, C. and J. R. C. van der Maarel. 2006. Plasmid DNA encapsulation within cationic diblock copolymer vesicles for gene delivery. J. Phys. Chem. B 110: 14550-14556.

6. Boles, T. C., J. H. White, and N. R. Cozzarelli. 1990. Structure of plectonemically supercoiled DNA. J. Mol. Biol 213: 931-951.

7. Bednar, J., P. Furrer, A. Stasiak, J. Dubochet, E. H. Egelman, and A. D. Bates. 1994. The twist, writhe and overall shape of supercoiled DNA change during counterion-induced transition from a loosely to a tightly interwound superhelix. Possible implications for DNA structure in vivo. J. Mol. Biol 235: 825-847.

8. Lyubchenko, Y. L., and L. S. Shlyakhtenko. 1997. Visualization of supercoiled DNA with atomic force microscopy in situ. Proc. Natl. Acad. Sci. U S A 94: 496-501.

9. Hammermann, M., Brun, N., Klenin, K. V., May, R., Tóth, K. and Langowski, J. 1998. Salt-dependent DNA superhelix diameter studied by small angle neutron scattering measurements and Monte-Carlo simulations. Biophys J 75: 3057-3063.

10. Zakharova, S. S., Jesse, W., Backendorf, C., Egelhaaf, S. U., Lapp, A., van der Maarel J. R. C. 2002. Dimensions of plectonemically supercoiled DNA. Biophys J 83: 1106-1118.

11. Jacrot, B. 1976. The study of biological structures by neutron scattering from solution. Rep Prog Phys 39: 911-953.

12. Groot, L. C. A., M. E. Kuil, J. C. Leyte, J. R. C. van der Maarel, J. -P. Cotton, and G. Jannink. 1994. Partial structure functions of DNA

fragment solutions; concentration effects. J. Phys. Chem 98: 10167-10172.

13. Boue, F., Cotton, J. P., Lapp, A., Jannink, G. 1994. A direct measurement of the polyion conformation in aqueous solutions at different temperatures small – angle neutron scattering of PSSNa using zero average and full contrast. J Chem Phys 101: 2562-2568.

14. Kassapidou, K., Jesse, W., M. E. Kuil, A. Lapp, S. Egelhaaf, and J. R. C. van der Maarel. 1997 Structure and charge distribution in DNA and poly(styrenesulfonate) aqueous solutions. Macromolecules 30: 2671-2684.

15. Higgins, J. S., Benoit, H. C. 1994. Polymers and neutron scattering. Oxford university press, Oxford, UK.

16. Forsyth, V. T., Myles, D., Timmins, P. A., Haertlein, M. 2001. Possibilities for the exploitation of biological deuteration in neutron scattering, in J. Dianoux (Ed) Opportunities for Neutron Scattering in the 3rd Millennium (Institut Laue Langevin publication) pp: 4754.

17. Laux, V., Callow, P., Svergun, D. I., Timmins, P. A., Forsyth, V. T., Haertlein, M. 2008. Selective deuteration of tryptophan and methionine residues in maltose binding protein: a model system for

neutron scattering. Eur Biophys J 37: 815-822.

18. Artero, J. B., Haertlein, M., McSweeney, S., Timmins, P. A. 2005. A comparison of refined Xray structures of hydrogenated and perdeuterated rat Ecrystallin in H_2O and D_2O. Acta Cryst D 61: 1541-1549.

19. Di Costanzo, L., Moulin, M., Haertlein, M., Meilleur, F., Christianson, D. W. 2007. Expression, purification, assay, and crystal structure of perdeuterated human arginase I. Arch Biochem Biophys 465: 82-89.

20. Wood, K., Frölich, A., Paciaroni, A., Moulin, M., Härtlein, M., Zaccai, G., Tobias, D. J., Weik, M. 2008. Coincidence of dynamical transitions in a soluble protein and its hydration water: Direct measurements by neutron scattering and MD simulations. J Am Chem Soc 130: 4586-4587.

21. Sandberg, L. M., Bjurling, A., Busson, P., Vasi, J., Lemmens, R. 2004. Thiophilic interaction chromatography for supercoiled plasmid DNA purification. J. Biotechnology 109: 193-199.

22. Backendorf, C., Olsthoorn, R., van de Putte, P. 1989. Superhelical stress restrained in plasmid DNA during repair synthesis initiated by the UvrA, Bprotein and Cproteins in vitro. Nucleic Acids Res 17:

10337-10351.

23. Shure, M., Pulleyblank, D. E., Vinograd, J. 1977. The problems of eukaryotic and prokaryotic DNA packaging and in vivo conformation posed by superhelix density heterogeneity. Nucleic Acids Res 4: 1183-1205.

24. van der Maarel J. R. C., Kassapidou, K. 1998. Structure of short DNA fragment solutions. Macromolecules 31: 5734-5739.

25. Lim, W., Ng, S. Y., Lee, C., Feng, Y. P., van der Maarel J. R. C. 2008. Conformational response of supercoiled DNA to confinement in a nanochannel. J Chem Phys 129: 165102.

26. de Vries R. 2005. Evaluating changes of writhe in computer simulations of supercoiled DNA. J Chem Phys 122: 064905.

27. Fujimoto, B. S., Brewood, G. P., Schurr, J. M. 2006. Torsional rigidities of weakly strained DNAs. Biophys J 91: 4166-4179.

28. van der Maarel J. R. C. 2008. Introduction to Biopolymer Physics. World Scientific, Singapore.

29. Rybenkow, V. V., Vologodskii, A. V., Cozzarelli, N. R. 1997. The effect of ionic conditions on the conformations of supercoiled DNA. I. Sedimentation analysis. J Mol Biol 267: 299-311.

30. Rybenkov, V. V., Vologodskii, A. V., Cozzarelli, N. R. 1997. The effect of ionic conditions on the conformations of supercoiled DNA. II. Equilibrium catenation. J Mol Biol 267: 312-323.

31. Fenley, M. O., Olson, W. K., Tobias, I., Manning, G. S. 1994. Electrostatic effects in short superhelical DNA. Biophys Chem 50: 255-271.

32. Schlick, T., Li, B., Olson, W. K. 1994. The influence of salt on the structure and energetics of supercoiled DNA. Biophys J 67: 2146-2166.

33. Vologodskii, A. V., Cozzarelli, N. R. 1995. Modeling of long-rangeelectrostatic interactions in DNA. Biopolymers 35: 289-296.

34. Gebe, J. A., Delrow, J. J., Heath, P. J., Fujimoto, B. S., Stewart, D. W., Schurr, J. M. 1996. Effects of Na+ and Mg2+ on the structures of supercoiled DNAs: comparison of simulations with experiments. J Mol Biol 262: 105-128.

35. Ubbink, J., Odijk, T. 1999. Electrostatic-undulatory theory of plectonemically supercoiled DNA. Biophys J 76: 2502-2519.

Chapter 5

Conclusions and future work

5.1 Conclusions

This thesis includes two main research aspects and addresses several issues of DNA solutions. A comprehensive characterization with particle video tracking of the viscoelasticity of solutions of rigorously monodisperse DNA with increasing concentration through the entanglement transition in terms of viscous loss and elastic storage moduli was presented. To study the conformation of supercoiled DNA, we have measured the small angle neutron scattering from pHSG298 plasmid as a function of plasmid and salt concentration. The distance between the two opposing duplexes of supercoiled DNA was determined. Our main research findings are listed as follows:

1. **Viscoelasticity of entangled phage λ-DNA solutions**

In order to investigate the dynamical properties of DNA, a comprehensive characterization of the viscoelasticity of DNA solutions was given. With increasing frequency, the viscous loss modulus first increases, then levels off, and eventually increases again. Concurrently, the elastic storage modulus

monotonously increases and eventually levels off to a constant high frequency plateau value. The elastic storage modulus becomes larger than the viscous loss modulus in an intermediate frequency range once the DNA molecules become entangled. The number of entanglements per chain is obtained from the high frequency plateau value of the elasticity modulus. The longest, global relaxation time is obtained from the low shear viscosity as well as from the lowest crossover frequency of the viscous loss and elastic storage moduli. The concentration dependencies of the low shear viscosity, the number of entanglements per chain, and the relaxation time agree with the relevant scaling laws for reptation dynamics of entangled polyelectrolytes in an excess of simple, low molecular weight salt with screened electrostatic interactions.

2. The effect of crowding on the conformation of supercoiled DNA from neutron scattering measurements

Small angle neutron scattering experiments were carried out in the condition of full and zero average DNA contrast using hydrogenated plasmid and a 1:1 mixture of hydrogenated and perdeuterated plasmid, respectively. For the first time, zero average DNA contrast was realized by the availability of perdeuterated plasmid. In the condition of zero average contrast, the scattering intensity is directly proportional to the single DNA molecule scattering function, eliminating complications from intermolecular interference.

It was observed that the interduplex distance (the distance between the two opposing duplexes in supercoiled DNA) decreases with increasing concentration of salt as well as plasmid. The crowding effect is highly sensitive to the salt concentration and is most significant in the condition of minimal screening. Therefore, besides ionic strength, DNA crowding is shown to be important in controlling the interwound structure and site-juxtaposition of distal segments of supercoiled DNA. The site-juxtaposition of distal DNA segments of supercoiled DNA in a crowded state such as in the cytoplasm of bacteria might have implications for gene regulation. This study also shows that at high DNA concentration, the intermolecular interaction is mainly determined by excluded volume, rather than screened electrostatics. Note that due to the lack of good models describing intermolecular organization of supercoiled DNA, we have refrained from further interpretation of the structure factor in terms of, e.g., the random phase approximation and virial coefficients.

5.2 Recommendation of future research

There are many interesting issues which could be explored in the area of molecular transport and structure of DNA in a congested state. An understanding of bio-molecules in crowded conditions is important to broad research fields. A few possible further studies based on this thesis are listed as

follows:

1. **DNA-protein interactions in relation to viscoelsticity**

In the area of dynamic properties of DNA, an overall characterization of the viscoelasticity of solutions of rigorously monodisperse DNA with increasing concentration in terms of viscous loss and elastic storage moduli was presented. The particle tracking method which requires only minute samples of no more than 15 μl each (1, 2) is particularly promising for the investigation of biological samples. More research could be done to study DNA-protein interactions by investigating the viscoelasticity in the presence of bacterial protein such as H-NS and HU (3, 4, 5). Different interactions between DNA and protein might give different viscoelasticity behaviors. In particular, the formation of transient networks by cross-linking protein can be gauged from the frequency scaling of the viscoelastic moduli.

2. **Dimensions of plectonemically supercoiled DNA under zero average contrast**

The zero average contrast method has successfully been applied before to investigate the structure of synthetic polyelectrolytes (6, 7). The effect of DNA crowding on the conformation of supercoiled DNA was investigated in this thesis for the first time. However, the DNA concentration and/or the superhelical density are not high enough to achieve a liquid crystalline phase.

It was reported that the radius and pitch decrease significantly with increasing plasmid concentration, covering the transition to the liquid crystalline phase (8). The present work contribute the decrease in radius, but possible changes in pitch were beyond observation due to limited signal strength. Further work using solutions of higher DNA concentration and simulations employing a nemelic potential might highlight such changes in molecular conformation.

3. Effect of crowding by nanoparticles and/or architectural protein

Zhang *et al*. investigated the effects of the generic crowding agent dextran on the structure and condensation of single DNA molecules in a nanochannel (9). It was observed that the DNA molecules elongate and eventually condense into a compact form with increasing volume fraction of the crowding agent. To further study the effect of crowding, it would also be possible to measure the interduplex distance of supercoiled DNA in the presence of a crowding agent, such as nanoparticles (dextran) through small angle neutron scattering. Instead of investigating single DNA molecules in a nanochannel (9), the effect of molecular crowding in the presence of dextran can be studied in the bulk phase.

Besides the possible studies mentioned above, the inclusion of proteins, *e.g.* H-NS and/or HU, in the neutron scattering measurements of DNA would be interesting and important to understand the DNA-protein interaction. Such

neutron scattering experiments can be achieved with the help of a combination of contrast variation techniques. Since neutron scattering measurements are best to study size-related properties of bio-molecules in solution, it would be also possible to pursue the effect of crowding on the conformation of bio-molecules, closer to the native state.

Reference

1. Goodman, A., Tseng, Y., and Wirtz, D. 2002. Effect of length, topology, and concentration on the microviscosity and microheterogeneity of DNA solutions. J Mol Biol 323: 199-215.
2. Mason, T. G. 2000. Estimating the viscoelastic moduli of complex fluid using generalized Stokes-Einstein equation. Rheol. Acta 39: 371.
3. Dame, R. T., Wyman, C. and Goosen, N. 2001. Structural basis for preferential binding of H-NS to curve DNA. Biochimie 83: 231-234.
4. Dame, R. T., Wyman, C. and Goosen, N. 2000. H-NS mediated compaction of DNA visualized by atomic force microscopy. Nucleic Acids Res 28: 3504-3510.
5. Liu, Y. J., Chen, H., Kenney, L. J., Yan. J. 2010. A divalent switch drives H-NS/DNA-binding conformations between stiffening and bridging model. Genes & Development 24: 339-344.
6. Boue, F., Cotton, J. P., Lapp, A. and Jannink, G. 1994. A direct measurement of the polyion conformation in aqueous solutions at different temperatures - small angle neutron scattering of PSSNa using zero average and full contrast. J. Chem. Phys 101: 2562-2568.
7. Kassapidou, K., Jesse, W., M. E. Kuil, A. Lapp, S. Egelfaaf, and J. R.

C. van der Maarel,. 1998. Structure and charge distribution in DNA and poly(styrenesulfonate) aqueous solutions. Macromolecules 30: 2671-2684.

8. Zakharova, S.S, Jesse, W., Backendorf, C., S. U. Egelhaaf, A. Lapp and J. R. C. van der Maarel, 2002. Dimensions of plectonemically supercoiled DNA. Biophys J 83: 1106-.

9. Zhang, C., Shao, P.G., Jeroen A. van Kan, and Johan R. C. van der Maarel., 2009. Macromolecular crowding induced elongation and compaction of single DNA molecules confined in a nanochannel. PNAS 39: 16651–16656.